THE DEVELOPMENT OF AN EFFICIENT TAKE-OFF PERFORMANCE MONITOR (TOPM)

R. Khatwa

The National Aerospace Laboratory NLR
Anthony Fokkerweg 2
1059 CM Amsterdam, The Netherlands

Abstract

The accident record indicates a need to improve take-off and initial climb safety. Factors adversely affecting performance can result in the scheduled accelerate-stop distance being exceeded even before the decision speed is reached, or the climb performance thereafter would be insufficient and unsafe. Current cockpit instrumentation is unable to positively detect these dangers. A Take-Off Performance Monitor (TOPM) could assist the pilot in keeping the progress of the take-off constantly in view, so as to make it easier to decide if a take-off can safely be continued, or to support the decision to abandon it. This paper considers the development of a TOPM with a predictive capacity. A pre-take off module calculates and displays the critical take-off lengths using nominally correct data. These lengths are evaluated on the basis of measured data and 'forward computations' during ground roll. Techniques to deal with anomalies such as sensor failures, incorrect data inputs, improper aircraft configuration and changes in take-off conditions during ground roll are proposed. The possibility of enhancing situation awareness by monitoring of engine health and acceleration performance is investigated. Consideration is also given to the nature and cockpit position of the display.

Nomenclature

A	Cross-sectional area of exhaust nozzle exit	m^2
a	Speed of sound	m/s
b_a	Accelerometer bias	m/s^2
b_G	Ground speed sensor bias	m/s
b_α	Gyroscope drift-rate bias	rad/s
C_D, C_L, C_M	Airplane drag, lift and pitching moment coefficient	
C_f	Nozzle coefficient	
C_{f0}, C_{f1}, C_{f2}	Polynomial coefficients	
D	Aerodynamic drag	N
F	nxn continuous system dynamics matrix	
F_G	Measured gross thrust (single engine)	N
F_m, F_n	Tyre friction force for main and nose gear	N
F_N	Net thrust (single engine)	N
G	nxr plant noise input matrix	
g	Acceleration due to gravity	m/s^2
H	mxn measurement matrix	
h_{cg}	Vertical distance from cg to force vector created by the tyres in contact with the runway	m
i_r	Inclination of thrust vector to x body-axis	rad
K	nxm Kalman gain matrix	
L	Aerodynamic lift	N
l_c	Current airplane position on runway	m
l_{VRc}	Predicted runway position for V_R speed	m
l_{VRm}	Limiting runway point for achieving rotation speed	m
l_{v1}	Predicted runway position for V_1 speed	m
l_0	Runway brake-release position	m
l_1	Ground roll distance to V_1	m
l_2	Ground roll distance from engine failure at V_1 to V_R	m
l_3	Runway distance from V_R to V_{LO} with one engine-out	m
l_4	Ground distance required to accelerate from V_{LO} to V_2 at screen height with one engine-out	m
M_∞	Mach number	
M	Airplane pitching moment	Nm
m	Airplane mass	kg
N_B	Number of braked wheels	
N_m	Total number of main gear wheels	
P	Static pressure	N/m^2
P	Tyre pressure	N/m^2
P	nxn covariance matrix of $\hat{\underline{x}}$	
P'	nxn covariance matrix of $\underline{x}'$	
P_t	Total pressure	N/m^2
P_{te}	Total pressure at nozzle exit	N/m^2
$Q(k)$	rxr system noise covariance matrix	
$Q(t)$	rxr spectral density matrix	
R	mxm measurement noise covariance matrix	
R_m, R_n	Main and nose gear reaction force	N
R_e	Earth equatorial radius	m
S	Wing area	m^2
S_c	Stopping distance required from current speed	m
S_{v1}	Predicted stopping distance from V_1 speed	m
T	Static temperature	K
T_N	Total net thrust (all engines)	N
T_{te}	Total temperature at nozzle exit	K
t	Time	s
t_{rs}	Time at which reverse thrust is selected	s
u	x-axis or North direction velocity	m/s
u_{rwy}	Inertial velocity in runway along track direction	m/s
V_{LO}	Lift-off velocity	m/s
V_P	Hydroplaning speed	m/s
V_R	Rotation speed	m/s
V_T	True airspeed	m/s
V_1	Decision speed	m/s
V_2	Take-off safety speed	m/s
v	y-axis or East direction velocity	m/s
$\underline{v}$	m-dimensional Gaussian measurement noise vector	
W	Airplane weight	N
w	z-axis velocity	m/s
$\underline{w}$	r-dimensional Gaussian plant noise vector	
w_a	Accelerometer white Gaussian noise	m/s^2

Symbol	Description	Units
w_G	Ground speed sensor white Gaussian noise	m/s
w_α	Gyroscope drift-rate white Gaussian noise	rad/s
X_{rm}, X_{rn}	Moment arm of main and nose gear reaction force	m
$\underline{x}$	n-dimensional state vector	
Z_T	Effective moment arm for all engines	m
$\underline{z}$	m-dimensional measurement vector	
α	Angle of attack	rad
Γ	nxr system noise coefficient matrix	
γ	Specific heat ratio	
γ_F	Flight path angle	rad
$\Delta l_{v1}, \Delta l_{vR}$	Contingency lengths	m
Δt	Sampling time	s
Δt_{rs}	Time between deploying lift dump and reversers	s
Δt_{sp}	Time interval between brake application and lift dump	s
ΔV	Discrete ground speed error measurement	m/s
$\Delta\dot{v}, \Delta\dot{u}, \Delta\dot{w}$	East, North and vertical accelerometer errors	m/s^2
$\Delta\Theta, \Delta\varphi, \Delta\vartheta$	IRS platform axes misalignment error angles	rad
δ	Dirac delta function	
δ_{eng}	Engine throttle setting	deg
δ_{kl}	Kronecker delta function	
ε	Statistical expectation	
η_B	Brake system efficiency	
Θ	Angle of rotation about geographic East axis	rad
θ_B	Airplane body axis pitch angle	rad
θ_R	Runway heading	rad
θ_{rwy}	Runway gradient	rad
μ	Coefficient of friction	
μ_B	Coefficient of braking friction	
μ_R	Coefficient of rolling friction	
ρ	Gas density	kg/m^3
φ	Angle of rotation about geographic North axis	rad
ϑ	Angle of rotation about geographic vertical	rad
Φ	nxn discrete system state transition matrix	

Subscripts

B	Body axes
Bdry, Bwet	Braking on a dry/wet surface
E	Geographic East
F	Flight path axes
FRL	Fuselage reference line
G	GSS measurement
I	IRS measurement in platform axes
id	Ideal
M	Measured quantity
m	Main gear
max	Maximum value
N	Geographic North
n	Nose gear
rwy	Runway
sp	Spoiler
T	True airspeed
w	Wind
WDP	Wing design plane
Z	Vertical (down) direction
1,2,....9	Stations for engine flow
∞	Free stream conditions

1 Introduction

Civil aircraft accident statistics reveal that the percentage of hull losses suffered during take-off is generally higher than for most other flight segments (except landing), despite the relatively low exposure time[1]. Furthermore, it is evident that take-off and initial climb safety has not improved during the last two decades [1,2]. Pilot opinion sought during this study revealed that the common feelings of anxiety existed among aircrew about take-off decisions and the associated accelerate-stop problems. In addition, there has been much debate about take-off certification issues during recent years and a universal set of rules has yet to be established amongst the world's airworthiness authorities.

The take-off certification criteria and decision speed concept are intended to guarantee that the aircraft has an acceptable level of safety during any take-off. The decision speed, V_1, is the speed at which the pilot could react to an engine failure and either continue or reject the take-off using a minimum runway length in either event. The field length computations are based upon the assumption that aircraft acceleration to V_1 will be *normal* and that *maximum* braking will be applied during the abort manoeuvre. However, factors such as runway contamination, unexpected changes in wind conditions, incorrect aircraft weight, degraded engine performance and tyre failures can adversely affect both take-off and stopping performance. These anomalies are not uncommon in everyday civil operations and often occur without crew recognition. Consequently the scheduled accelerate-stop distance may be exceeded even before V_1 is reached. Between 1975 and 1986 RTOs accounted for half of all take-off accidents and 56% of fatalities in such occurrences[3,4]. Moreover, the accident record shows that catastrophic overrun accidents continue to occur, even when failures (for the most part, not engine failures) require the take-off to be rejected at speeds substantially below V_1. Between 1962 and 1978 over 25% of the overruns were attributed to RTOs initiated at a speed equal to or below V_1[5].

Poor acceleration performance to V_1 may also limit the later climb performance. It could be that a very long runway would allow for eventual approach to V_1 and lift-off, but the climb performance thereafter would still be insufficient and unsafe. One example is the crash of the Air Florida Boeing 737 after take-off from Washington Airport in January 1982[2]. Engine pressure probe blockage by ice and failure to use engine anti-ice gave rise to a false Engine Pressure Ratio (EPR) indication in the cockpit, and in this case resulted in application of a lower thrust level than required. The aircraft failed to accelerate and climb as desired and was unable to sustain flight. In all, 78 people were killed. Failure to RTO was cited as a direct cause of the accident.

During the take-off roll the pilot currently has no means except his instinct by which he can determine whether the performance is normal for the existing weight and engine setting. Although alternative decisions near V_1 are limited (ie GO or RTO) the consequences of an incorrect deci-

220

sion can be catastrophic. A device displaying additional information to the pilot which can assist him in keeping the progress of the take-off constantly in view, so as to make it easier to decide if a take-off can safely be continued or to support the decision to abandon it, even before he reaches V_1, is known as a Take-Off Performance Monitor (TOPM). These systems have the potential to provide crucial performance information that is orientated towards the pilot's task during take-off.

Both the US National Transportation Safety Board and the UK Air Accidents Investigation Branch have continually advocated the need for improvements in take-off monitoring. Several accidents investigated by these bodies prompted increased attention to this need. Following the Air Florida accident the Society of Automotive Engineer's introduced an Aerospace Standard[2] to define TOPM system requirements. The FAA has itself recently outlined the necessary guidelines for approval of such systems[6].

Consideration has been given in the past to both distance-to-go runway markers and to time-to-speed checks to enable the pilot to make a GO/NO-GO judgement with regard to the aircraft acceleration up to the V_1 speed. Both methods have been discarded as insufficient for safe civil operations. Serious consideration was first given to take-off monitors when large jet transports were introduced into service, thus presenting the greater challenges of longer take-off runs and longer stopping distances. A large number of proposals were put forward which varied considerably in scope, methods of measurement and presentation of information to the pilot [7-9]. The idea most commonly proposed was the concept of comparing achieved and acceptable performance, for example acceleration monitoring[7]. Most systems were crude in nature and none received wide-spread approval for civil operations.

The attempts to provide pilots with take-off assistance has suffered from the inadequacies of technology in previous decades, if not from a careful consideration of the true needs of a pilot at one of the most critical moments in flight. Systems technology and integration has advanced at a rapid rate since the early programmes and the capacity to process large amounts of data quickly now suggests that TOPM development is a more feasible challenge.

A large proportion of the more recent efforts are aimed at implementing very simple instruments, without predictive features, on general aviation aircraft (for example Ref. 10). Systems proposed for larger transport aircraft have either not come to fruition or are still in the development stages[3,11-15]. These latter efforts are all generally aimed at providing the pilot with predictive assistance and consider both the continued take-off status and the stopping ability of the aircraft. Additional cues such as acceleration and engine health monitors are proposed in Ref. 3, 12. A more comprehensive review of previous TOPM studies is given in Ref. 3. Note that the author was previously involved in the Bristol University investigation[3] and some of what appears herein reflects ideas from that study.

Although much creditable work has been conducted recently, further studies are required to tackle outstanding issues before acceptability from both pilots and airworthiness authorities develops. This paper considers the development of an efficient TOPM with a predictive capacity, and identifies potential monitoring functions and the necessary algorithms which form the foundation of the displayed cues. The remainder of this paper is subdivided as follows. The principles of operation of a predictive TOPM are reviewed in Section 2. Section 3 deals with the data input process and computations executed prior to take-off. The processes required to filter flight data are considered in Section 4. The role and development of an Engine Performance Monitor are outlined in Section 5. Section 6 focuses on the processes required to deduce reliable predictions of the critical take-off lengths and acceleration monitoring concepts are considered in Section 7. The TOPM display format and cockpit position are briefly discussed in Section 8. Finally, the TOPM algorithms developed in this study are evaluated for a number of test cases in Section 9.

2 Principles of Operation of a Predictive TOPM

The SAE Aerospace Standard[2] identifies any TOPM by TYPE. The definitions are summarised below.

TYPE I   Type I monitors compare the achieved aircraft performance to a reference performance based on all-engines at normal take-off power. These monitors have no predictive capability.

TYPE II   Type II monitors have all the capabilities of Type I monitors, but in addition have the ability to predict performance later in the take-off run.

TYPE III   This Type of monitor has all Type I and Type II capabilities and also can continuously predict the ability of the aircraft to abort take-off.

The virtues of the various TOPM Types are discussed in Ref. 3, 14. It is likely that the predictive capacity of a TOPM is crucial to flight safety if only because considerable warning would be given before a critical situation developed. Predictive monitors help eliminate the split-second decision making process. Type III systems provide information that is more orientated towards the task the pilot is expected to perform during take-off. Thus the remainder of this paper considers the development of a monitor which is at least as comprehensive as the requirement for Type III.

The layout of the take-off reference speeds relative to the runway end are shown in Fig. 1. For a realistic system specification, the proper requirements will have to take account of the following, namely the distances associated with stopping, or clearing the screen height with the critical engine-out, from the runway position at which a decision is made. For the TOPM there is a need to calculate the total length beyond a critical speed (V_1 or V_R) to clear the screen with a failed critical engine and to achieve an agreed V_2 based on current aircraft data, eg all-up-weight, for the climb performance required. The total distance required would involve a

calculation *backwards* from the screen height effectively. This length is a primary factor governing the GO/NO-GO decision.

The important requirements for a decision to support a safe take-off or abort might be met by the following variation. Fig. 2 shows a display which assumes that the aircraft joins the runway at some point near a taxiway and removed from the near end of the runway. The following parameters are illustrated

(a) the current aircraft position on the runway (l_c), a continually lengthening coloured bar (green) growing within a simple runway outline,
(b) stopping distance required for the current speed (S_c) (red bar),
(c) the runway position (l_{vRc}) at which a critical speed, say V_R, will be reached and indicating that the take-off 'can go' (a narrow bar across the runway strip, coloured (green) and visible as the 'next marker' along the strip),
(d) the position on the runway (l_{vRm}), calculated backwards from the screen or stopway, at which the same critical speed must be reached in order to satisfy the minimum safe take-off or safe abort requirements and at which the take-off 'must go'. (Another narrow bar (red) and initially visible beyond the 'next marker'.)

These critical lengths must be displayed on the basis of real measured data and forward computations. For Type III monitors there are three basic segments central to the development of the TOPM, namely pre-takeoff module, establishing current take-off conditions and the predictive computations[3,12].

The relative positions of the two warning bars 'can go' and 'must go' will provide predictive assistance to the pilot. These bars would migrate if the take-off parameters changed during the ground roll. As the two bars associated with l_{vRc} and l_{vRm} close upon each other, the pilot's margin for error, delay or decision narrows and if the order of the two bars is reversed, ie the pilot sees the red bar as the 'next marker' along the runway strip, he can forsee problems before they arise. Take-off can be aborted before a threat to safety arises.

2.1 The definition of sufficient warning
It is debatable whether or not there is great virtue in presenting the length S_c which is not of great interest until it grows toward equality with the stopping distance required from V_1. Indeed one has to make a case for the *sufficiency* of the reverse calculation from V_2 to V_R to establish the last point at which both options are open to the pilot. If both the stopping distance and the continued take-off distance required are displayed on the simulated runway strip, a small segment of that strip could become cluttered and confusing.

The balanced field length calculation requires the distances associated with continuing take-off to a height of 35 feet after engine failure at V_1, and the distance to stop from the decision speed, to be equal. The equivalence of the two lengths assumes that stopping distance has

been calculated with valid friction data. These could change and it can be argued that instead of a reverse calculation of the length given in Fig. 1 from V_2, a comparable reverse calculation should be made from the end of the stopway, to find the requirement for runway remaining at the latest decision point. Whichever criterion is used, there can be displayed a 'must go' position on the runway strip and, for convenience, only one such position is shown on Fig. 2, namely l_{vRm}.

3 Pre-Takeoff Module

The TOPM must possess pre-takeoff capacity in order to accept input data defining the current conditions, establish nominal parameters demanded by the real-time segment, and estimate the critical take-off lengths prior to brake-release.

3.1 Data requirements
The one-time system inputs belong to one of four categories, namely ambient conditions, aircraft configuration and payload data, runway information and take-off reference speeds. The data requirements are summarised in Table 1. Entry of aircraft configuration and payload data could almost certainly be automated on modern transport aircraft by exploiting subsystems such as the Flight Management System (FMS) and the Weight and Balance System (WBS). Details of the runway could be entered into the TOPM manually, but in a mature system they would probably be available *via* an Electronic Library System (ELS). The entry of runway condition would be governed by the formal definitions in JAR 25 AMJ 25X591[16] and a selection of one of the following would be made

· dry
· wet
· standing water, slush or loose snow
· compacted snow
· wet ice.

This particular input allows the TOPM to select the appropriate braking characteristics for predicting stopping distances. Details of the braking friction data are given in Section 6.2.

3.2 Atmospheric properties
The reported ambient conditions enable a calculation of the air density, speed of sound, and temperature and pressure ratios. These parameters are required to execute airplane performance calculations and evaluated using standard ideal gas equations[3].

3.3 True reference airspeeds
The take-off reference speeds (namely V_1, V_R, V_{LO}, V_2) normally obtained from the flight manual calculations are calibrated airspeeds (CAS) and must be transformed into true airspeeds (TAS) for manipulation by system algorithms. This is accomplished by use of standard compressible flow equations[3].

3.4 Thrust estimation
Airplane performance calculations inevitably require a knowledge of the engine thrust characteristics. The thrust data is determined by employing an empirical model of the steady state behaviour of the engine, together with standard

table-look-up procedures[3,12]. The primary variables are ambient temperature and pressure, Mach number and throttle setting, thus

$$F_N = f(M_\infty, T_\infty, P_\infty, \delta_{eng}) \quad . \tag{1}$$

The net thrust is then established as a function of Mach number for the current ambient conditions and recommended throttle setting. This enables thrust to be deduced by virtue of a simple one-dimensional table-look-up during the real-time segment.

Data similar to that for forward thrust may be generated for reverse thrust in order to estimate stopping distance. To be consistent with certification criteria, credit for reverse thrust should be given only in those instances where regulations allow it[3].

3.5 Nominal acceleration performance
This element of the pre-takeoff module generates the airplane's acceleration performance as a function of the true airspeed for three values of the friction coefficient, namely the nominal pilot input, an unusually low value 0.005 and a higher than normal value 0.04. This acceleration-airspeed data is used for the real-time distance-to-go predictions. The choice of the friction coefficient values is justified in Section 9. The instantaneous forces and moments acting on the airplane during ground roll are illustrated in Fig. 3. A detailed aircraft model (which includes aerodynamic, engine and landing gear models) performs these computations. The aircraft trimming routine and dynamic model outlined in Ref. 3,12 are suitable for this purpose. Fig. 4 is an example of the output from this block of the pre-takeoff module.

3.6 Nominal data for real-time predictions
A number of parameters, both constant and time varying, are governed by the current aircraft configuration and required by the real-time computations. The gear force moment arms (X_{Rn} and X_{Rm}) about the cg and the vertical distance from the cg to the force vector created by the tyres (h_{cg}), as established by the airplane trimming routine, are used as nominal values for real-time predictions. The nominal airplane lift, drag and pitching moment coefficients (C_L, C_D, C_M respectively) for the selected flap and horizontal stabiliser settings are established. The increments in lift, drag and pitching moment coefficients ($\Delta C_{L_{sp}}, \Delta C_{D_{sp}}, \Delta C_{M_{sp}}$ respectively) with full spoiler deflection are also computed (as a function of the flap deflection). Factors such as ground effect and increments for the landing gear are accounted for when evaluating the aerodynamic coefficients.

3.7 Prediction of take-off distances
The performance algorithms incorporate factors such as actual runway profile and degraded braking characteristics associated with runway contaminants. Tyre rolling frictional forces are based on the nominal coefficient of rolling friction. Stopping predictions must include the effects of reverse thrust for those aircraft whose scheduled take-off data are based on the deployment of reversers. The algorithms outlined in Section 6 are employed to estimate the critical distances above (with the appropriate initial conditions). Thus those take-offs that are predicted to be only marginally safe would become apparent.

Note the critical runway position l_{vRm} is calculated as the difference between the total runway length and the distance ($l_3 + l_4$) shown in Fig. 1. An outboard engine is assumed to fail at V_1. A detailed analysis of the dynamic response to asymmetric power usually involves both longitudinal and lateral equations, but when the failure occurs just prior to take-off, and initial recovery actions have been applied, a simple analysis employing only the longitudinal equations of motion which allows for factors such as thrust loss, windmilling drag and rudder drag yields reasonable results[3]. This approach has been adopted herein. Distances l_3 and l_4 are estimated by assuming a step input of the elevator at V_R, and the numerical integration of the dynamic equations continues to the screen. The undercarriage is assumed to remain fully extended and the dynamic airplane model referred to in Section 3.5 is used to determine the flight profile. The incremental drag coefficient due to rudder deflection is evaluated using an iterative procedure; the rudder angle is altered until the side force yawing moment generated is equal in magnitude to that due to asymmetric thrust[3].

3.8 Reference acceleration data
It is sufficient to note at this stage that data for the reference acceleration monitor (referred to in Section 7) is established during this block of the pre-takeoff calculations.
Note that most of the pre-takeoff calculations could alternatively be performed by ground based computers with the relevant data down-loaded prior to take-off.

4 Current Take-Off Conditions

The problem of establishing current take-off conditions is one of processing aircraft sensor data. This section considers the processes required to filter the flight data, the algorithms to deal with redundant data sources (an excess of sensors), and the isolation of faulty sensors.

4.1 Data sources
Whilst conventional sources of data such as the Inertial Reference System (IRS) and the Air Data Computer (ADC) are bound to be used, alternative sources such as rotation servos in the wheel units and perhaps a reflective method such as forward looking doppler or a mechanism akin to a radio altimeter directed toward highly reflective targets at each runway threshold could be employed. Various engine related parameters, for example throttle position, EPR and exhaust nozzle temperature could be used not only for setting take-off power, but also for monitoring engine health[3]. The use of a Tyre Pressure Indicating System (TPIS) could prove to be a useful warning device. It is recognised that the selection of sensors normally available onboard would depend upon the aircraft type in question. The Boeing 747 aircraft model employed in the investigation at Bristol University is assumed to house the following, namely an IRS, alternative ground speed sensor (GSS), an ADC and a TPIS.

223

4.2 Signal selection and reliability

The degree of hardware redundancy required for TOPM implementation would ultimately be governed by reliability requirements. The requirements in Ref. 2 stipulate that with a Built-In-Test-Equipment (BITE) confidence test, the probability of system failure during *take-off* must be reduced to less than 10^{-3}. However, the JAR 25 requirements are more stringent. If the effect of TOPM failure is considered as Minor by JAR 25.1309[16], then the corresponding target probability is set as 10^{-5} per *flight hour*.

Signal selection algorithms are required to deal with redundant data sources and with the isolation of faulty sensors, thus reducing redundancy and inevitably changing reliabilities. Traditional methods of fault tolerant sensor operation involve voting among sensors of the same type. For example, with three perfect like sensors the signal selector chooses the mid-value for use in the algorithms. When operating on dual sensors the fault detection and isolation module compares the moving window average of the difference of two signals against a predetermined threshold prior to signal selection time. For two perfect sensors the average of the signals is transmitted to the algorithms.

4.3 Filtering of flight data

Suitable filters must be employed as state estimators because of the uncertainties involved in the sensor outputs. The type of filter implementation utilised would be determined by the number of independent measurements available for a particular parameter. Parameters that are required continuously during the real-time segment include

- along-track acceleration from the IRS
- ground speed from the GSS
- TAS and CAS from the ADC
- engine temperatures and pressures.

Outputs from the ADC and engine sensors are processed by a digital low-pass filter. The filter was implemented as a first-order transfer function and modelled in the discrete domain by utilising the Bilinear Transformation[3].

4.3.1 Sensor data blending

Filtering methods can provide the most likely value from a few differing sources of the same nominal signal, for example the blending of IRS and GSS ground speeds. Superior estimates of the take-off conditions also enhance the accuracy of the predictive performance routines. A fixed-gain Complementary Filter is utilised in Ref. 12 to blend GSS and IRS signals in order to deduce accurate acceleration estimates. The application of a Kalman Filter to obtain optimal estimates of the take-off conditions using a similar sensor set has also been investigated[17]. That approach is considered herein. The objectives in applying Kalman Filtering to the data gathering for a TOPM are, at least

- production of reliable 'best estimates' when a particular variable might be available from more than one source and thus available with instantaneously different values.
- Improvements on basic signals which are subject to errors from hardware with known dynamical operations.

In applying the Kalman Filtering theory to the TOPM problem, the 'indirect' approach is used in which the error states of the dynamic process are estimated. These error states are used to correct the outputs of the navigation systems in a feedforward mechanisation to produce best estimates of the take-off conditions. See Fig. 5. The filter is then based on statistical error models for each of the systems involved.

The IRS considered herein employs the geographic axes (ie East, North and vertical) as the reference frame for measurements and we assume that the platform is not aligned correctly with the geographic axes; the East, North and vertical platform stabilising gyroscopes are in error by angles $\Delta\Theta$, $\Delta\varphi$ and $\Delta\vartheta$ respectively. It is assumed that the GSS provides measurements in the runway reference frame. The data from the motion sensors must be processed by filter algorithms in a common frame of reference; the appropriate transformation matrix between platform variables and the runway reference frame must be computed[3]. The relationship between geographic, platform and runway axes is shown in Fig. 6. For this investigation it has been assumed that the runway along-track direction is aligned with geographic North and the aircraft is constrained to move along a meridian of a non-rotating Earth. The IRS will then indicate directly the acceleration along the runway and the East velocity is taken to be zero.

4.3.2 Kalman Filter algorithm

The mathematical model of the plant used in the Kalman Filter is assumed to be a Markov process defined by the following difference equation

$$\underline{x}(k+1) = \Phi(k+1,k)\underline{x}(k) + \Gamma(k)\underline{w}(k) \ . \tag{2}$$

The discrete observations are given by

$$\underline{z}(k) = H(k)\underline{x}(k) + \underline{v}(k) \ . \tag{3}$$

The noise processes $\underline{w}$ and $\underline{v}$ are assumed to be uncorrelated zero-mean Gaussian white-noise sequences. The noise statistics are

$$\varepsilon\{\underline{w}(k)\} = 0 \quad \varepsilon\{\underline{v}(k)\} = 0 \quad for \ all \ k$$

$$\varepsilon\{\underline{w}(k)\underline{w}^{T}(1)\} = Q(k)\delta_{k1}$$

$$\varepsilon\{\underline{v}(k)\underline{v}^{T}(1)\} = R(k)\delta_{k1}, \quad R(k) > 0 \ . \tag{4}$$

Assume, also, that the state vector initial condition, $\underline{x}(0)$, is uncorrelated with respect to $\underline{w}$ and $\underline{v}$. The best estimate of the state, $\hat{\underline{x}}(k+1)$, and its variance, $P(k+1)$, at time t_{k+1} can be updated for minimum variance by the following Kalman update equations[18].

Time update

$$\underline{x}'(k+1) = \Phi(k+1,k)\hat{\underline{x}}(k) \tag{5}$$

$$P'(k+1) = \Phi(k+1,k)P(k)\Phi^{T}(k+1,k) + \Gamma(k)Q(k)\Gamma^{T}(k) \tag{6}$$

224

Measurement update

$$K(k+1) = P'(k+1)H^T(k+1) [H(k+1) \\ P'(k+1)H^T(k+1) + R(k+1)]^{-1} \quad\quad (7)$$

$$\underline{\hat{x}}(k+1) = \underline{x}'(k+1) + K(k+1)[\underline{z}(k+1) - H(k+1)\underline{x}'(k+1)] \quad (8)$$

$$P(k+1) = P'(k+1) - K(k+1)H(k+1)P'(k+1) \quad\quad (9)$$

with initial conditions

$$\underline{\hat{x}}(0) = \varepsilon\{\underline{x}(0)\}$$

$$P(0) = \varepsilon\{[\underline{x}(0) - \underline{\hat{x}}(0)][\underline{x}(0) - \underline{\hat{x}}(0)]^T\} \quad .$$

It is well known that round-off errors inherent in the implementation of the filter equations on a finite word-length digital computer can give rise to filter divergence[19]; the covariance matrix ceases to be positive definite and symmetric. The square root formulation of the filter circumvents this difficulty by computing the square root of P (and P') instead of P and thereby cuts in half the number of significant figures required of the computer. The algorithm due to Schimdt[19] to compute the time update of the covariance matrix and the Andrews[20] square root formulation for the measurement update of the covariance matrix have been employed in the filter design. Alternatively, Bierman's well known UD factorisation method could be used.

4.3.3 State equations for the filter

The error in a state is defined as the indicated value minus the true value. As an example, only simple models of the sensor uncertainties are used in this study. Typical IRS errors would be accelerometer biases, platform tilt errors, gyro drift and white Gaussian noise. The minor effects of gyro drift during take-off are included here for completeness. The tilt error introduces components of 'g' and vertical acceleration, $\dot{w}_I$, in the accelerometer measurement aligned with the North axis. It is assumed here that $\dot{w}_I$ can be measured with negligible error. As $\Delta\theta$ is small, the effect of a measurement $\dot{w}_I$ corrupted with noise and biases will be negligible. The gyro drift-rate error model is assumed to consist of a bias component and a white noise process. A similar error model is employed for the GSS measurement. The stochastic linear system model for the error states may be written in matrix form as[17]

$$\begin{bmatrix} \Delta\dot{u}_I \\ \Delta\dot{x} \\ \Delta\dot{\theta} \\ \dot{b}_a \\ \dot{b}_\alpha \\ \dot{b}_G \end{bmatrix} = \begin{bmatrix} 0 & 0 & (\dot{w}_I - g) & 1 & 0 & 0 \\ 1 & 0 & 0 & 0 & 0 & 0 \\ -1/R_e & 0 & 0 & 0 & 1 & 0 \\ 0 & 0 & 0 & 0 & 0 & 0 \\ 0 & 0 & 0 & 0 & 0 & 0 \\ 0 & 0 & 0 & 0 & 0 & 0 \end{bmatrix} \begin{bmatrix} \Delta u_I \\ \Delta x \\ \Delta\theta \\ b_a \\ b_\alpha \\ b_G \end{bmatrix} + \begin{bmatrix} 1 & 0 \\ 0 & 0 \\ 0 & 1 \\ 0 & 0 \\ 0 & 0 \\ 0 & 0 \end{bmatrix} \begin{bmatrix} w_a \\ w_\alpha \end{bmatrix}$$

$$(10)$$

ie $\quad \underline{\dot{x}}(t) = F(t)\underline{x}(t) + G(t)\underline{w}(t) \quad .$

The error measurement at discrete time intervals is

$$\Delta V = u_I - u_G = \Delta u_I - \Delta u_G \quad\quad (11)$$

$$= [1\ 0\ 0\ 0\ 0\ -1] \begin{bmatrix} \Delta u_I \\ \Delta x \\ \Delta\theta \\ b_a \\ b_\alpha \\ b_G \end{bmatrix} - w_G \quad\quad (12)$$

ie $\quad \underline{z}(t) = H(t)\underline{x}(t) + \underline{v}(t) \quad .$

For the purpose of practical implementation on a digital computer the continuous state-space form model defined above requires to be converted to the equivalent discrete-time model. It is well known that for small sampling intervals Δt

$$\Phi(t_{k+1}, t_k) = e^{\Delta t\, F(t_k)} = \sum_{n=0}^{\infty} \frac{\Delta t^n}{n!} F^n(t_k) \quad\quad (13)$$

where $\quad \Delta t = t_{k+1} - t_k \quad .$

The covariance matrix of the random sequence $\Gamma(k)\underline{w}(k)$ is

$$\Gamma(k)Q(k)\Gamma^T(k) = \int_{t_k}^{t_{k+1}} \Phi(t_{k+1}, \tau)G(\tau)Q(\tau)G^T(\tau)\Phi^T(t_{k+1}, \tau)\,d\tau$$

$$(14)$$

where $Q(t)$ is the spectral density matrix. An approximate solution of this integral for small Δt is easily found by substituting the expansion for the Φ matrix.

In order to initiate the Kalman Filter, it is necessary to specify an initial state estimate, $\underline{\hat{x}}(0)$, and its associated a priori covariance matrix, $P(0)$. This covariance matrix is simply a diagonal matrix consisting of the variances of the individual initial state error variances. The initial estimate of the state variables were assumed to be

$$\underline{\hat{x}}(0) = [0\ 0\ 0\ 0\ 0\ 0]^T \quad . \quad\quad (15)$$

All terms required by the filter are now defined and the Kalman equations can be used to estimate the errors in the measurement signals. As only the scalar measurement case is presented here the appropriate simplifications (eg matrix inversion avoided) have been made in the implementation.

4.3.4 Failure and error checks

The Kalman filter can diverge in the presence of hardware failures. This may be detected by monitoring and checking the calculated variance in the filter and the mean and standard deviation of the innovation process[18]. A simple failure modes and effects analysis conducted suggests that when items of data are suddenly withdrawn due to hardware failure, the Kalman state estimator cannot always be expected to behave satisfactorily[3]. Thus alternative algorithms should be employed so that the TOPM continues to function, but with degraded performance. If either the IRS or GSS function completely fails then the system reconfigures to utilise a low-pass filter to process the remaining signal. A high-

pass filter *(pseudo differentiator)* is used to deduce acceleration from GSS measurements of velocity. (These latter signals, as expected, are somewhat noisy even when a high filter time constant is employed.) Further details are given in Ref. 3.

5 Engine Performance Monitoring (EPM)

In practice take-off field lengths and decision speed computations are based upon the acceleration of the aircraft assuming normal take-off power. Improper power setting and sub-standard thrust development have both contributed to previous take-off accidents. One of the primary pilot tasks during take-off is the monitoring of engine health. Typically, the crew is presented with filtered sensor data such as EPR or the low pressure compressor rotational speed rather than an indication of actual thrust. Current caution and alerting systems do not necessarily detect degraded engine conditions. It is also known that several factors which give rise to sub-standard thrust are not reflected in the EPR measurement, eg engine intake icing, foreign object ingestion and intake temperature variations. Consequently the crew is not always able to positively detect sub-standard thrust, as in the Air Florida case.

Engine sensor data processed and presented in a form that is more directly related to the pilot's task could potentially reduce both pilot workload and the associated errors[21]. An enhanced Engine Monitoring and Control System (EMACS)[21], which presents total engine performance information (including a display of actual thrust), was recently evaluated against a traditional electronic engine display in a flight simulator. Results confirm the substantially superior failure detection abilities of EMACS. It is interesting to note that the Air Florida engine anomaly was included in the evaluation and detected by pilots only when presented with the EMACS display.

An enhanced EPM could potentially aid the GO/NO-GO judgement. The EPM could also communicate with TOPM stopping prediction algorithms so that the extent of the engine/reverser malfunctions are accounted for[22]. A thrust measuring system suitable for real-time engine health monitoring is considered below.

5.1 Thrust method options
A universal method for determining in-flight thrust does not exist at present. Several method options exist involving varying degrees of effort, complexity and accuracy. Most techniques belong to one of four categories[3,23], namely trunnion thrust, swinging probe, overall performance and gas-path methods. The first two methods have had limited application to date because of the number of drawbacks, eg complexity of the installation, arranging for accurate measurements. Overall performance methods employ curves or tables that describe average engine performance in terms of an engine operating parameter. However, the disadvantage of these methods is that they assume all relevant influences have been accounted for. If, for example, the engine flight environment differs from that of the ground tests, or ageing occurs, then the actual thrust developed would differ from the calibrated value.

Gas-path methods rely on measurements taken within the engine to enable flow conditions to be calculated at various engine stations using mass, momentum and continuity principles. The flow characteristics are related to thrust through calibration of the engine and nozzle in a ground/altitude facility. The number of method options available is large and in practice need to be assessed for a particular case. Two gas-path methods that have been extensively investigated and proven to be feasible and accurate are the Mass Momentum Method (MMM) and the Simplified Gross Thrust Method (SGTM)[24]. The relative simplicity of these methods allows the gross thrust to be computed in real-time, with accuracy comparable to the much slower and more complex traditional Gas Generator Methods. As an example, the MMM implementation is considered herein.

5.2 Mass Momentum Method
The general concept of the MMM (and SGTM) is to relate real nozzle performance to that of an ideal nozzle through use of empirically established coefficients. The nozzle thrust coefficients are usually functions of nozzle pressure ratio and nozzle geometry. Nozzle coefficients account for factors such as[23] the three-dimensional nature of the flow, real gas effects, dissociation of real gases and mass flow leakage.

5.3 Thrust calculations
The MMM essentially determines the force caused by the change in momentum of the fluids passing through the engine. The general equations to calculate the thrust of an ideal convergent nozzle are determined using one-dimensional isentropic flow relationships for two flow conditions, namely subcritical (unchoked) and supercritical (choked). Only the final equations are presented here, the reader is directed to Ref. 3,24 for the derivations. The nozzle is considered unchoked whenever

$$\frac{P_{te}}{P_\infty} < \left(\frac{\gamma + 1}{2}\right)^{\frac{\gamma}{\gamma-1}}$$

and the appropriate thrust equation is

$$F_G = \frac{2A_e P_\infty \gamma C_f}{\gamma - 1}\left[\left(\frac{P_{te}}{P_\infty}\right)^{(\gamma-1)/\gamma} - 1\right]. \qquad (16)$$

Alternatively, for choked nozzle flow

$$\frac{P_{te}}{P_\infty} \geq \left(\frac{\gamma + 1}{2}\right)^{\frac{\gamma}{\gamma-1}}$$

and the basic thrust equation is

$$F_G = C_f A_e \left[\left(\frac{2}{(\gamma + 1)}\right)^{\gamma/(\gamma-1)}(\gamma + 1)P_{te} - P_\infty\right]. \qquad (17)$$

5.4 Instrumentation
Inspection of Equations 16 and 17 reveals that the EPM demands measurements of only the total pressure in the nozzle and the ambient static pressure. A twin-spool turbofan engine model (see Fig. 7) with a thrust rating similar to

that of a Rolls Royce RB-211 has been employed in this study. Since both streams in a turbofan engine provide contributions to the total thrust, it is necessary to provide pressure measurement instrumentation in both the hot core and the fan exhaust flows. If isentropic flow is assumed, then the low pressure turbine (LPT) discharge total pressure (P_{t7}) and the total pressure in the by-pass duct (P_{t3}) fulfill the requirements of Equations 16 and 17. In many engines, probes of this type are already present, at least in the core flow as part of the EPR measurement system. Sufficient instrumentation (number of probes or rakes) is required to obtain representative mean pressures over the intended range of engine operating conditions. Sensors must be oriented to allow for the errors that will occur if the engine design or the installation of the sensors themselves causes substantial radial or circumferential flow components. The uncertainty of a measurement may be reduced by employing voters to eliminate bad measurements. All measurements are processed by a low-pass filter network prior to entering the EPM algorithms. Instrumentation characteristics are considered fully in Ref. 23.

Note that for both the unchoked and choked flow conditions

$$\gamma = f(T_{te}) \ . \tag{18}$$

The preferred procedure is to use real gas properties, whereby γ is obtained from tables as a function of the exhaust gas temperature. Thus additional instrumentation is required, but measurement of at least the exhaust gas temperature in the core flow is available onboard most turbofan aircraft. However, a constant γ has been adopted elsewhere and its effect corrected by the nozzle coefficient[24]. This approach has been adopted herein; values of γ equal to 1.3 and 1.4 for core and by-pass streams respectively.

Note that as all pressure probes are located downstream of rotating machinery, thrust measurement accuracy is not affected by combustion degradation or intake distortion.

5.5 Nozzle coefficients
The gross thrust coefficient is defined as the ratio of the actual thrust to ideal thrust obtained from an ideal nozzle at a given pressure ratio, ie

$$C_f = \frac{F_{G_M}}{F_{G_{id}}} \ . \tag{19}$$

The thrust measurements are usually made on a ground thrust calibration facility. A series of engine tests are conducted at various power settings and the data are collected up to the available nozzle pressure ratio. For higher nozzle pressure ratios available in flight, the data are either extrapolated or more accurate data are obtained using an altitude test facility.

Flight test data were not available for this investigation and an equivalent theoretical means of estimating the empirical coefficients was employed. The twin-spool turbofan employed for this study was operated at numerous conditions to establish the likely range of nozzle pressure ratios to be encountered during the take-off. A second-order polynomial curvefit was then performed on the data so that

$$C_f = C_{f0} + C_{f1}NPR + C_{f2}(NPR)^2 \tag{20}$$

where NPR is the nozzle pressure ratio and C_{f0}, C_{f1}, C_{f2} are the polynomial coefficients. Coefficients were established for both core and by-pass flows.

5.6 Reference gross thrust
In order to detect possible malfunctions the EPM must compare actual thrust developed with that expected from a healthy engine. The inputs to the reference gross thrust module must be indicative of the aircraft flight speed and ambient conditions for the current (measured) power setting. The reference thrust can be deduced from the empirical engine model outlined in Section 3.4. The exact location of the malfunction cannot be established by the EPM alone as the thrust is the integrated output of all powerplant sub-assemblies. Other measured parameters would be required to localise the problem source.

The process above can only confirm satisfactory operation of the engine for the *current* throttle setting and does not have the ability to detect sub-standard thrust due to incorrect power setting for the prevailing conditions. (eg In the case where the pilot incorrectly selects a low power setting the engine would function satisfactorily in the absence of anomalies.) As an additional check, the measured thrust is also compared with the thrust expected for the flight manual recommended take-off power setting.

6 Prediction Algorithms

Fundamental to the objectives of this research is the desire to produce a display with reliable predictive capacities which will provide warnings of take-off dangers earlier than would otherwise be the case. This section focuses on the processes required to deduce estimates of these predictions.

The rolling resistance characteristics of the runway need to be established, including impingement drag associated with runway contaminants. Runway contaminants will affect braked wheels and friction coefficients cannot be assumed to remain unchanged for stopping performance predictions. The TOPM algorithms will need to take into account the extent of engine or tyre failures and the consequential effect on the aircraft's performance. Other anomalies such as excess weight and incorrect control settings unknown to the pilot must also be reflected in all performance computations in order to avoid misleading the crew. The current windspeed as obtained from an onboard windspeed estimator should be incorporated in all predictions such that dangerous situations arising from unexpected wind changes are prevented. The accuracy of the prediction phase would be enhanced if the actual runway profile rather than the official effective gradient were employed.

6.1 Distance-to-go predictions

A feature which has encouraged opposition to the introduction of the TOPM in the past is the uncertainty in the friction coefficient assumed for contaminated runways. The variable values of tyre rolling resistance can give rise to inaccurate predictions. Such predictions could introduce unnecessary RTOs or even fail to warn the pilot of an approaching emergency.

Research into the friction characteristics of aircraft tyres, summarised in Ref. 25,26 (and references therein), has established that in general the rolling friction coefficient (μ_R) is a function of at least

- forward speed
- tyre pressure
- surface contaminant
- footprint area
- vertical load
- tyre heating
- runway surface.

For example, μ_R increases with increase of forward speed at constant load and tyre pressure. In addition, softer runway surfaces give rise to a higher rolling resistance. For dry surfaces the larger the footprint area, the larger the value of μ_R[26]. Experience indicates that μ_R decreases in magnitude on a damp runway relative to the dry surface value. For slush and water covered runways the retardation force increases parabolically with increasing forward velocity and approximately linearly with depth and density of the contaminating fluid. Further retardation forces are caused by the slush spray impingement on the aircraft surfaces.

These studies provide a large volume of friction data to permit determination of empirically derived equations and relationships for use in estimating a particular tyre friction performance. However, it is not always possible to find values of μ_R for the particular combination of conditions of interest. A method to determine μ_R for *actual* conditions at any point during the ground roll would enhance the accuracy of the predictions and thus result in a more reliable monitor. The analysis in Ref. 26 shows that if the ground roll distance is needed to within an inaccuracy of 5%, then μ_R should be estimated to within 50%.

The instantaneous forces acting on the airplane during the ground roll are illustrated in Fig.3. Ignoring the pitching motion a simple resolution of the forces yields

$$m\dot{u}_{rwy} = T_N\cos(i_r) - D - W\sin\theta_{rwy} - \mu_R$$
$$(W\cos\theta_{rwy} - L - T_N\sin(i_r)) \ . \qquad (21)$$

The approach adopted in this study is to estimate an *effective friction coefficient* which involves combining measurements from the aircraft sensors with Equation 21. This equation is rearranged so that

$$\hat{\mu}_R = \frac{\hat{T}_N\cos(i_r) - \hat{D} - \hat{W}\sin\hat{\theta}_{rwy} - \frac{\hat{W}}{g}\hat{\dot{u}}_{rwy}}{\hat{W}\cos\hat{\theta}_{rwy} - \hat{L} - \hat{T}_N\sin(i_r)} \qquad (22)$$

where the dressing '$\hat{\ }$' denotes estimated values. The aircraft weight, W, can either be a manual pilot input or ideally be acquired from a WBS. Filter outputs contribute values of the sensed parameters, ie longitudinal acceleration from the Kalman or Complementary Filter whereas the ADC provides the TAS. The output of the ADC is usually ignored at low speed ($\simeq$ 45 knots) due to ill-conditioning in air data equations. In this regime the airspeed may be estimated as the sum of the filtered ground speed and reported windspeed component along the runway, ie

$$\hat{V}_T = \hat{u}_{rwy} + \hat{u}_W \qquad (23)$$

and the corresponding Mach number is

$$\hat{M}_\infty = \frac{\hat{V}_T}{\hat{a}_\infty} \qquad (24)$$

where $\hat{a}_\infty$, the estimated speed of sound, is computed by the pre-takeoff module.

The lift and drag forces are computed by employing the nominal aerodynamic coefficients and the estimated air density ($\hat{\rho}_\infty$) generated during the pre-takeoff computations

$$\hat{L} = \frac{1}{2} \hat{\rho}_\infty\hat{V}_T^2 \ S \ C_L$$
$$\hat{D} = \frac{1}{2} \hat{\rho}_\infty\hat{V}_T^2 \ S \ C_D \ . \qquad (25)$$

The net thrust developed is estimated for the recommended take-off static EPR by virtue of a simple table-look-up, ie

$$\hat{T}_N = f(EPR, \hat{M}_\infty) \ . \qquad (26)$$

Runway gradient is deduced by a table-look-up and is stored as a function of the runway position, ie

$$\hat{\theta}_{rwy} = f(\hat{x}_{rwy}) \ . \qquad (27)$$

In the low speed domain where the ADC output is considered unsatisfactory the reported windspeed conditions are employed but thereafter the difference between the filtered ADC airspeed and filtered ground speed are used to estimate the wind velocity vector. Substitution of the quantities above into Equation 22 enables the effective friction coefficient to be estimated.

A prediction of the distance to achieve any critical speed from current conditions is accomplished by employing a standard Euler numerical integration technique[3]. Having established the effective friction coefficient using Equation 22, the acceleration for the mean velocity of each integration speed interval is deduced by linearly interpolating between the acceleration-airspeed curves generated by the pre-takeoff module. Ten speed intervals were used for the integration.

6.2 Prediction of stopping distance

An emergency-stop schedule that complies with JAR 25 (illustrated in Fig. 8) can be adopted to predict stopping distance. Assume that the pil-

ot applies the retarding devices in the following order: maximum footbrakes, close throttles, deploy spoilers and apply reverse thrust. The fundamental elements of this prediction are considered below.

6.2.1 Equations of motion

The component retarding forces acting on the airplane during the braked roll consist of the rolling resistance, aerodynamic drag, engine ram drag, engine reverse thrust (if employed) and braking force. Fig. 9 shows a simplified arrangement of these forces. The analysis assumes nominal values for the length h_{cg}, and landing gear force moment arms X_{rm} and X_{rn} (computed during the pre-takeoff segment). Consider prediction of stopping distance S_c. Assuming an equivalent main landing gear of two struts[3] and resolving forces perpendicular to the runway surface gives

$$2R_m + R_n + L - W\cos\theta_{rwy} = 0 \qquad (28)$$

ignoring the thrust vector contribution. The friction force developed at the main wheel-runway interface is limited either by braking friction coefficient or by the brake system torque limit. For the friction-limited case, taking moments about the cg results in

$$M + T_N Z_T + R_n X_{rn} - 2R_m|X_{rm}| - \mu_n R_n h_{cg} - 2\mu_m R_m h_{cg} = 0 \quad (29)$$

which may be rearranged as

$$R_n = \frac{M + T_N Z_T - 2R_m|X_{rm}| - 2\mu_m R_m h_{cg}}{\mu_n h_{cg} - X_{rn}} \qquad (30)$$

and substituting this into (28) yields

$$R_m = \frac{(W\cos\theta_{rwy} - L)(\mu_n h_{cg} - X_{rn}) - M - T_N Z_T}{2(\mu_n h_{cg} - X_{rn} - |X_{rm}| - \mu_m h_{cg})} \cdot \qquad (31)$$

Having established R_m, R_n can then be estimated by use of Equation 28, ie

$$R_n = W\cos\theta_{rwy} - L - 2R_m \cdot \qquad (32)$$

Resolving along the runway gives

$$\frac{W}{g}\frac{dS_c}{dt} = T_N - D - W\sin\theta_{rwy} - \mu_n R_n - 2\mu_m R_m \cdot \qquad (33)$$

A similar analysis for the torque limited case yields

$$R_m = \frac{(W\cos\theta_{rwy} - L)(\mu_n h_{cg} - X_{rn}) - M - T_N Z_T + 2F_{m_{max}} h_{cg}}{2(\mu_n h_{cg} - X_{rn} - |X_{rm}|)} \qquad (34)$$

$$\frac{W}{g}\frac{dS_c}{dt} = T_N - D - W\sin\theta_{rwy} - \mu_n R_n - 2F_{m_{max}} \qquad (35)$$

where $F_{m_{max}}$ is the maximum force that each brake unit is able to generate. The effects of the various retarding devices are discussed below.

6.2.2 Wheel braking forces

A theoretical method to determine the braking friction coefficient (μ_B) does not exist at the present time, but it is known that the friction coefficient developed is affected by factors such as[3]

· tyre load
· tyre size, tread, temperature and pressure
· type of runway surface and contamination
· airplane velocity
· tyre or wheel slipping velocity
· brake torque capacity
· manner of brake application.

6.2.2.1 Tyre factors

There is no evidence to suggest that tyre diameter affects the coefficient of friction available on wet or dry surfaces[3,27]. For dry surfaces μ_B is independent of the tyre tread pattern, whereas for wet pavements factors such as location of grooves, groove width and rib width influence the braking force. These factors are interrelated but a general treatment of their effects is difficult. In general, tyres with circumferential ribs will develop significantly higher friction forces than smooth tyres[27]. For both wet and dry runways μ_B usually decreases with increase in tyre inflation pressure[27].

6.2.2.2 Runway surface factors

For dry conditions the available data indicate no significant effect of changes in surface texture. For wet runways the effects of variations in surface texture on μ_B are appreciable. In general, smoother micro-textured pavements result in a lower level of friction. For wet surfaces the available friction force is also governed by the amount of water on the runway. On slush-covered runway surfaces values of μ_B are usually lower than on water-covered surfaces, whereas the braking performance on ice-covered runways is generally poorer than on surfaces contaminated with snow. Runway traction on snow- or ice-covered surfaces is extremely variable and depends primarily upon temperature of the air and runway surface, the condition of the snow (loose or packed), and the presence of a water film on the packed snow or ice. Hydroplaning can also occur on a flooded or slush-covered runway.

6.2.2.3 Aircraft and operational factors

In general the magnitude of μ_B decreases with increase in forward speed. For wet surfaces the friction coefficient decreases as the tyre wears. For both wet and dry surfaces the effect of changes in normal tyre load on μ_B is minor[27].

6.2.2.4 Braking friction coefficient data

Accurate friction coefficient data are essential for assessing the braking capability of an aircraft. The results of investigations aimed at developing empirical methods for predicting aircraft tyre friction performance from ground-vehicle braking tests appear to be satisfactory. For example, Ref. 28 outlines a technique of deducing braking friction coefficients of an aircraft main gear tyre from diagonal-braked vehicle friction measurements. However, Ref. 29, 30 imply that such studies have not necessarily succeeded in presenting an accepted approach to predicting the stopping of an aircraft with any certainty. Determination of aircraft tyre fric-

tion performance, however, is difficult at best considering the varied influence of both tyre and runway characteristics, and the effects of brake system performance.

A large volume of experimental friction data for aircraft tyres under various conditions of speed, load, etc is available to estimate braking performance, for example, Ref. 27 (and references therein). The arguments above and elsewhere[27] suggest that data for μ_B in dry conditions show no appreciable effects of changes in surface texture, tyre tread pattern and tyre diameter. For dry runway surfaces μ_B is dependent primarily on forward speed and tyre pressure. The following expression is derived from the empirical data presented in Ref. 27 for a tyre pressure of 300 lbf/in^2

$$\mu_{Bdry} = 0.623 - 1.708E^{-3} \, \hat{u}_{rwy} \, . \tag{36}$$

(Note that $\hat{u}_{rwy}$ above is in m/s). For wet conditions data are presented in Ref. 27 as a function of speed and tyre pressure for several surface textures. Friction coefficients are included for rib and smooth tread tyres. Thus for any particular tyre tread and inflation pressure only a modest number of curves needs to be stored for use by the TOPM, ie the problem is reduced to one of relating the two prime variables of speed and surface texture.

Current airworthiness criteria, in particular JAR 25 AMJ 25X1591[16], contain wheel braking characteristics to enable estimation of stopping distance on a variety of contaminated runway surfaces, namely *dry*, *wet*, *standing water*, *slush*, *loose snow*, *compacted snow* and *ice*. In the absence of flight test data specific to a particular aircraft type, tyre, braking system and runway contaminant these approved data could be employed. This approach has been adopted for the proposed design. The following data are presented in AMJ 25X1591.

(a) *Wet runway*. The braking friction is derived by use of data presented in Table 2, ie the product of the factor μ_{Bwet}/μ_{Bdry} and μ_{Bdry} (Equation 36) at a given speed. In addition the magnitude of μ_{Bwet} derived by this technique is not permitted to exceed 0.4.

(b) *Standing water, slush or loose snow*. If V_P is the estimated hydroplaning speed then

$$\mu_B = 0.25\mu_{Bdry} \quad \text{for} \quad \hat{u}_{rwy} \leq 0.9V_P$$

$$\mu_B = 0.05 \quad \text{for} \quad \hat{u}_{rwy} > 0.9V_P \, . \tag{37}$$

The classical equation (where P, the tyre pressure, is in lb/in^2 and V_P is in knots) for estimating the hydroplaning speed is

$$V_P = 9\sqrt{P} \, . \tag{38}$$

(c) *Compacted snow*. Assume a value of μ_B equal to 0.2.

(d) *Wet ice*. A braking friction coefficient of 0.05 should be adopted.

Fig. 10 illustrates the variation of these data as a function of ground speed.

6.2.2.5 Brake system efficiency

Operation of the wheel brakes at the optimum slip ratio would produce the highest aircraft deceleration, but in practice the effective value obtained is appreciably less because of brake application technique. The actual value of the friction coefficient generated is governed by the brake system efficiency (η_B) and thus

$$\mu = \eta_B \, \mu_B \, . \tag{39}$$

The magnitude of η_B depends primarily on the type of brake system and values of between 0.6 and 0.9 are common for anti-skid systems; a value of 0.8 is adopted herein. In practice, the manufacturer's data should be exploited.

6.2.2.6 Total friction coefficient developed

As only main gear wheels are assumed to possess braking capacity the friction coefficients developed are

$$\mu_n = \mu_R \tag{40}$$

$$\mu_m = \mu_R + \eta_B \, \mu_B \, . \tag{41}$$

In fact the latter equation could be rewritten in the more general form

$$\mu_m = \mu_R + \frac{N_B}{N_m} \, (\eta_B \, \mu_B) \tag{42}$$

where N_B and N_m represent the number of braked wheels and the total number of main gear wheels respectively. A TPIS (to monitor tyre health) could give indications of N_B and consequently allow better estimates of stopping distance. Note that a tyre failure is necessarily associated with an increase in rolling drag. No attempt is made here to incorporate this factor into the stopping predictions.

It is assumed that braking commences after the legal two-second time delay and that the brakes then become fully effective in a ramp fashion per given period of time[3,12].

6.2.3 Spoiler activation

Assume that spoiler movement is initiated (Δt_{sp} + 1) seconds after wheel brake application, Δt_{sp} being the time interval between the completion of brake application and initiation of the spoiler movement demonstrated during certification; the additional one second is a legal requirement. The change in the incremental coefficients $\Delta C_{L_{sp}}$, $\Delta C_{D_{sp}}$ and $\Delta C_{M_{sp}}$ from zero (at zero spoiler deflection) to the values for maximum spoiler deflection is represented by a first-order lag. The increments deduced from this process are added to the nominal aerodynamic coefficients.

6.2.4. Thrust schedule

Throttle closure is assumed to be initiated immediately after the two-second mandatory delay period. Engine 'spin down' is represented by a first-order lag.

Current UK requirements allow credit for the use of reverse thrust, in contrast to US FAR which do not. Assume that reverse thrust is selected $(\Delta t_{rs} + 1)$ seconds after completion of the actions required to deploy spoilers, where Δt_{rs} is the certification demonstration time to conduct the same manoeuvre. The reverse thrust schedule used herein includes[3]

- a time delay for reverser actuation; a linear transition with time
- engine acceleration back up to speed; first-order lag
- time at maximum reverse thrust
- engine deceleration after reaching a prescribed cutoff groundspeed (20 m/s); first-order lag.

The reversers are selected at time

$$t_{rs} = 4 + \Delta t_{sp} + \Delta t_{rs} . \qquad (43)$$

Ground idle thrust is assumed to exist after the thrust decay following reverser cancellation. Note that during each of these phases the EPM could ensure that credit for reverse thrust is withdrawn if failures are detected[3].

The thrust reverser effects on lift, drag, and pitching moments must be accounted for; appropriate incremental coefficients are added to the equations for C_L, C_D and C_M[3].

6.2.5 Solution of the equations of motion

The aerodynamic forces and moments, thrust, aircraft mass, current estimated windspeed, runway gradient (Equation 27), and friction force are required in the point-mass performance calculation (Equations 31-35) to estimate the aircraft acceleration. An Euler integration scheme is employed to compute the stopping distance and terminates operation when the ground speed reaches zero; the appropriate initial conditions must be specified. Initial values of acceleration, velocity, runway position, TAS and current windspeed are demanded by this algorithm.

7 Acceleration Monitoring

It has long been argued that the capacity to detect a significant performance deficiency can be encompassed by employing an acceleration monitor. A common proposal has been the comparison of measured acceleration with the nominal value deduced from the equations of motion for the reported conditions. The advantage of this simple monitor is its immediate reaction to abnormalities such as engine failure[3,12]. The disadvantage is that it cannot relate a deficiency in acceleration to the runway length, the distance already gone, and the previous history of the take-off, so as to discriminate properly between safe and unsafe situations[3]. The danger is that some take-offs may be considered sub-normal while the performance would still be within acceptable limits. Thus these concepts have faced considerable opposition from airworthiness authorities in the past.

Consider the following. In general one of two conditions will prevail prior to brake-release, namely

(a) the minimum distance required to rotate and climb-out to the screen with engine failure, $(l_3 + l_4)$, is greater than the stopping distance required from V_1,

(b) S_{v1} is greater than $(l_3 + l_4)$.

Both (a) and (b) above are illustrated in Fig. 11. The parameters Δl_{vR} and Δl_{v1} represent the contingency spaces respectively. Thus in case (a) the aircraft is able to suffer a performance loss provided the total distance to V_R does not exceed l_{vRm}. Similarly for case (b) a performance loss equivalent to a length Δl_{v1} can be tolerated before a critical situation arises. Calculation of the lengths l_{vRm} and S_{v1} enables the limiting factor (a) or (b) above to be established. An iterative scheme can be employed in which the magnitude of the friction coefficient is sufficiently increased (ie acceleration reduced) so that the critical speed (V_1 or V_R depending on which is the limiting criterion) is achieved at the limiting point[3]. This value of the friction coefficient, hereinafter referred to as the *reference friction coefficient*, can be employed to deduce the *reference acceleration* by use of the airplane acceleration-airspeed data generated during the pre-takeoff segment. The reference acceleration thus represents the minimum performance level required to conduct both the GO and STOP manoeuvres on the current runway.

During the ground roll the take-off conditions may change and thus the limiting criteria (a) or (b) above may be reversed. For example loss of braking capacity is associated with multiple tyre failure and thus an increase in the length S_{v1}. Parameters such as tyre and engine health could be continuously monitored (*via* TPIS and EPM respectively) and the limiting criteria reestablished in the presence of any failures. If the limiting criterion is altered then the corresponding reference friction coefficient could be computed again.

Note that when there is an update on the reference friction coefficient the reference may be raised to a higher value under certain conditions[3]. This implies that the aircraft has been accelerating at greater than the reference value and therefore the runway distance covered up to the time of failure (and update) is less than the reference acceleration would have predicted. (So too would the distances necessary to achieve V_1 or V_R be less than those predicted with the reference acceleration.) As a consequence, the iterative procedure described above yields an updated reference friction coefficient whose magnitude is greater than before. Thus the aircraft can suffer a greater performance loss than would have seemed allowable before. It could even be argued that the reference friction coefficient should be continuously updated in real-time and under normal operating conditions a steadily increasing value would be deduced. However, with this scheme it is likely that only very severe performance degradations would be detected.

In the present implementation the updated friction coefficient is employed for monitoring purposes only if its magnitude is smaller than the pre-takeoff segment value. This would represent a *greater* constraint on the maximum allowable value and would lead to a *higher* requirement for

acceleration, ie the policy was conservative. If the updated value for a reference friction coefficient had been larger than that from pre-take-off calculations, thus allowing lower accelerations for zero contingency in runway length, then circumstances such as an engine failure could produce a highly undesirable situation. Further details are given Ref. 3.

8 Nature and Position of the Display

Current regulations regarding TOPMs require the nature of the display to provide only *advisory* information to the crew as opposed to *commanding* a rejected or continued take-off[2,6]. The runway strip presentation employed herein illustrates concept only and in practice the optimum nature and position of the display must be established. However, this would not materially affect the development of the analytical and predictive algorithms which form the foundation of displayed cues. Rapid assimilation of the right information is crucial to good piloting during those very important few seconds prior to a GO/NO-GO decision.

It may be necessary to supplement the 'runway strip' presentation with an additional cue to alert the pilot of an approaching emergency or indeed to indicate that the take-off performance is satisfactory. These cues could employ the predictive techniques considered above and can take the form of advisory flags[3,12]. Discussions with pilots during this investigation suggest that a STOP flag may be ignored at high speed (especially close to V_1 on a distance limiting take-off) as the consequences of a maximum effort abort under these conditions are often brake heating, multiple tyre failure and fire, possibly followed by a runway overrun. It appears that a large proportion of pilots are go-minded at high speed[3]. Pilots involved in the NASA TOPM evaluation[13] indicated that the STOP option should not be displayed at high speed unless a generous safety margin is included in the stopping distance calculation. The stopping algorithms outlined herein respond to engine reverser and tyre failures in an effort to deduce more reliable predictions. However, Ref. 14 indicates that from a human factors point of view, rapidly changing display information at a time when the crew is expected to make instant decisions may not be ideal. It is suggested that the last abort position on the runway, allowing for a failure (engine or tyres), be displayed instead. Clearly a comprehensive human factors study is required to determine a widely acceptable solution to the display problem.

Whatever display is used for a TOPM, a modified display prior to take-off could lead the pilot *via* taxiways to the runway assigned by ATC. The full map would eventually be reduced to a large display of only one runway, namely that for the ground roll[3,4].

The cockpit position of the TOPM display is crucial; a position which falls within (or close to) current take-off instrument scan patterns would minimise distraction from currently defined procedures. On modern aircraft the TOPM display could appear on an existing Cathode Ray Tube (CRT) such as the Primary Flight Display (PFD) or the Navigation Display (ND). Available

space on the PFD is limited and thus the format of the TOPM display must be tailored to fit within existing constraints.

The location of head-down displays, such as those above, must be as high as possible on the instrument panel in order to minimise the scan angle between windshield and the CRT location; this allows the pilot to focus more of his attention on conditions ahead. The suggestion of a runway strip requires some concentration even in its simplest form and may be of real value only when the pilot-not-flying (PNF) regularly calls out useful advice to the pilot-flying (PF). It could well require too much head-down time and perhaps some form of Head-Up Display (HUD) should be employed instead. Pilot opinion sought during this study indicated a strong desire for a HUD.

The HUD may be of the peripheral type or of the collimated projected type. In the case of the former, information is presented in the pilot's peripheral vision so that he remains head-free. Perhaps little more than coloured lights driven by the predictive computing techniques may be sufficient as a cue. A simplified display visible to the pilot while he is head-up may even supplement a more complex head-down display. A simplified display of this type could enhance the situation awareness of the PF[13]. The projector type HUD enables the TOPM display to be presented on the windshield to both pilots.

Whatever the display position, it is clear that an appropriate pilot training programme and widely acceptable crew procedures must be developed prior to the introduction of any TOPM into civil operations. Human factors research together with real flight trials will be necessary before confidence can be gained in a truly useful scheme.

8.1 NLR display development

The NLR TOPM investigation is based on the fundamental philosophy that the pilot's most essential function is *to be in command*. This study involves both algorithm and display development as well as a reliability study[14,31]. Currently, human factors studies are being conducted to evaluate the concepts and displays associated with each of the three monitor Types. The goal is to establish the display Type which most effectively enhances the pilot's GO/NO-GO decision making process and to identify the necessary display information. In addition, pilot performance without a take-off monitor (ie the current situation) is also being investigated and thus the potential benefits of any monitor Type can be established; a traditional PFD is used as the basis of comparison. A Silicon Graphics IRIS work-station facility[31] employed to conduct this investigation is configured for a one-man crew. The work-station is interfaced with a control stick for pitch control and a throttle box for demanding changes in thrust. The advantages of using a work-station include the possibility of gathering data from a very large number of simulations and it also allows the use of non-pilot test subjects: comparison of performance with pilot subjects enables detection of possible pilot biases due to training and/or airline procedures. The test subjects are divided into three categories, namely twin-engi-

ned aircraft pilots, multi-engined aircraft pilots and non-pilots. Twin-engined aircraft pilots are being subjected to a Fokker 100 simulation, whereas multi-engined aircraft pilots are employed on a Boeing 747 simulation. The aircraft employed for all non-pilot tests is the Fokker 100.

Due to the complexity of the task an EPM has not been incorporated in the study. The three TOPM displays investigated are described below. (Note these displays are an updated version of those referred to in Ref. 14.)

8.1.1 Type I display
A simple form of a Type I display appearing on the PFD is shown in Fig. 12. The following are presented.

(a) Actual and scheduled airspeeds: the scheduled airspeed (*solid* yellow triangle) represents the airspeed which would normally be achieved at a given runway position for the reported conditions and the flight manual recommended engine setting. Any speed (performance) loss would cause the CAS (hollow) triangle to lag behind the scheduled airspeed marker.

(b) Speed-trend (magenta line) information indicating a five-second prediction of airspeed. A *reference speed-trend* (white cursor) based on a 15% reduction of the expected acceleration for the recommended power setting and reported conditions. Note that these cues provide a means of monitoring *inertial* acceleration.

(c) Current runway position of the aircraft (yellow). The tick marks represent 1000 ft positions.

In the event of an engine failure both the reference speed-trend and scheduled CAS symbols disappear from the display.

8.1.2 Type II display
The Type II display appears on the ND (see Fig. 13) and presents the following guidance.

(a) Current runway position of aircraft (yellow), plus 1000 ft markers.

(b) Predicted (ie *continuously* updated) and nominal (ie fixed point) runway positions which the aircraft will reach when its speed becomes V_R. These positions are represented by a yellow cross and blue circle respectively. The relative position of these two symbols indicates the extent of any adverse/favourable factors.

(c) The region on the runway (continuously updated) where a decision to continue take-off safely with an engine failure is possible. This is indicated by (blue) 'can go' bars.

If take-off conditions change such that the predicted V_R position marker migrates <u>beyond</u> the ground roll limit position (not displayed) then the colour of the marker changes from yellow to red, indicating a potentially dangerous continued take-off.

In the event of an abort the predicted V_R position symbol and the 'can go' bars disappear.

8.1.3 Type III display
The Type III TOPM is similar to the Type II display, but also presents the last runway position (continuously updated) from which it would be possible to conduct a safe stop (assuming no credit for reverse thrust). See Fig. 14. A safe stop is implied when the aircraft symbol appears between the (brown) 'can abort' bars. In the event of an abort the 'can abort' bars are *frozen* for the entire stopping manoeuvre. For the Type III display, TOPM information alone can be utilised to make the take-off decisions and thus V_1 speed data has not been furnished to pilots for these tests.

Both qualitative and quantitative data analysing techniques are being employed to assess each display Type. For example, aspects such as display dynamics, ease of interpretation, mental workload and situation awareness are being scrutinised. Other factors such as actions taken by the pilot (eg GO or RTO), reaction times and speed of detecting anomalies are also being investigated. Preliminary results indicate that a TOPM improves pilot detection of non-standard airplane performance. For example, Fig. 15 shows the response of all test subjects (for all test runs) to the on-line question "were there any non-standard factors present during take-off?" The final results of this study will be used to modify and optimise existing features of the most promising display Type, prior to implementation on the NLR Research Flight Simulator for further evaluation. This latter study will benefit from a more realistic cockpit environment, with both PF and PNF interaction.

9 Take-Off Monitor Algorithm Evaluation

The algorithms outlined above have been evaluated on the Bristol University IBM 3090 mainframe using a B-747 dynamic model and the appropriate sensor models (with their attendant errors and noise values)[3]. The real-time segment inputs are summarised in Table 3. Fig. 16 shows the TOPM processes in block diagram form. A sampling frequency of 20 Hz has been employed for the TOPM computations. As an example the results of three scenarios are presented below, followed by a summary of the main results of the investigation (full details in Ref. 3). The example simulations below were performed for standard sea-level conditions, assuming a horizontal runway and zero wind conditions. An aircraft mass of 320725 kg and cg location of 14% mean aerodynamic chord were selected for the time responses. Note that in all figures below the term *true friction coefficient* refers to the runway rolling friction coefficient employed in the full aircraft simulation and *measured acceleration* implies filter output values.

9.1 Dry runway
Fig. 17a shows the variation of four critical lengths with time, namely current aircraft position (l_c), distance to V_R for current conditions (l_{vRc} - l_c), distance to stop from current speed (S_c) and stopping distance required at V_1 (S_{v1}). The discontinuity in the S_c curve is due to reverse thrust activation. From Fig. 17b it is evident that the lengths (l_c + S_c) and (l_{v1} + S_{v1}) are always less than the runway length, thus indicating satisfactory take-off conditions. Fig. 17b also indicates that l_{vRc} is always

within the ground roll limit constraint, l_{vRm}, implying a safe climb-out. The estimation of distances l_{vRc} and l_{v1} is based on the nominal input of the rolling friction coefficient during the first five seconds (see Fig. 17c) and on the algorithm estimated value thereafter. The initial discrepancy between the estimate of l_{vRc} and the true position at which rotation is achieved (Fig. 17b) is due to the difference between the nominal rolling friction coefficient selected (ie 0.01) and the actual value of μ_R (0.02). This discrepancy decreases once real-time estimates of the effective friction coefficient become available and the error in the estimate of l_{vRc} grows to about -64 m (3.08%). Fig. 17c shows good agreement between estimated and true rolling friction coefficients. It is evident that the reference rolling friction coefficient is always greater than the estimated value, again indicating safe conditions. The large difference between measured and reference accelerations (and friction coefficients) is due to the non-limiting nature of the take-off. Thus the performance can fall below that required for normal operating conditions and the aircraft would still have the ability to take-off or stop safely. Note that measured acceleration falls slightly below the nominal acceleration (Fig. 17d); a direct consequence of employing a nominal value of μ_R smaller than the actual value. In general *exact* values of μ_R will not be available prior to take-off.

9.2 Thrust setting 15% too high

The effect of accidentally setting the take-off thrust at a level higher than that recommended by the flight manual is simulated here. Needless to say that performance would improve as clearly depicted in Fig. 18a and Fig. 18b. Referring to Fig. 18c it is evident that the estimated *effective friction coefficient* fluctuates about -0.02 whereas the true value of the *rolling friction coefficient* is 0.02. An excess amount of thrust is thus interpreted as a reduction in the friction coefficient and consequently this improves the accuracy of the distance-to-go predictions. An engine failure flag was not set as the engine functioned satisfactorily for the actual throttle setting. Thus the stopping predictions employed full available reverse thrust. The higher-than-normal thrust level was detected by the EPM. Fig. 18d shows that measured acceleration is higher than both nominal and reference accelerations.

9.3 Weight underestimated and engine failure

An increase in rolling drag and a decrease in the braking friction coefficient gives rise to longer critical take-off lengths l_c, l_{vRc}, S_c and S_{v1} as Fig. 19a shows. The benefits of applying reverse thrust also become more obvious. The distance-to-go predictions respond to excess weight and the engine failure as illustrated in Fig. 19b. In this example, the stopping predictions employ a lower level of reverse thrust after engine failure and the malfunction is detected by the EPM. However, the stopping predictions and the ground roll limit position computation are both based on the incorrect (lower) aircraft mass. A WBS could be employed to overcome this problem.

Fig. 19c indicates that prior to engine malfunction the estimated *effective friction coeffi-*

cient fluctuates about 0.65 whereas the magnitude of μ_R is 0.031. The excess weight has been attributed to an increase in friction coefficient. The parameter ($l_{v1} + S_{v1}$) is predicted to exceed the runway length (Fig. 19b), indicating an unsafe RTO from V_1. The estimated friction coefficient exceeds the reference value (Fig. 19c) and this implies sub-standard performance. Consequently the measured acceleration falls below the reference and nominal values as shown in Fig. 19d. However, at this time the relative positions of l_{vRm} and l_{vRc} (although very close) indicate that the continued take-off option is available. With engine failure the performance degrades even further, and as Fig. 19b shows the algorithm predicts that V_R can no longer be achieved before the limiting point. Fig. 19c shows a further step increase in the estimated friction coefficient at engine failure time. This new effective friction coefficient is a composite term accounting for both anomalies present. The algorithm evaluates a new reference friction coefficient at engine failure time and the magnitude decreases to -0.0175. This decrease is due primarily to the higher stopping distance required from V_1. The corresponding increase in the reference acceleration indicates that a greater threat to safety exists.

10.0 Summary of Results and Discussion

The distance-to-go predictions are able to account for a variety of anomalies that are encountered in everyday operations including

- engine failure/incorrect throttle setting
- tyre failure
- runway friction characteristics (eg dry, wet, contaminated)
- incorrect data input (eg ambient temperature, aircraft weight, control settings)
- incorrect loading (eg excess weight)
- incorrect control setting selected by the pilot for the prevailing conditions.

These anomalies are accounted for by the *effective friction coefficient* estimation procedure, whether acting singly or in combination. The simulations demonstrated that the distance l_{vRc} could be estimated in most cases to an inaccuracy of about 4%. For normal take-off performance the algorithm attempts to estimate the *rolling coefficient of friction*. During any period of performance deficiency the airplane acceleration is reduced and consequently the algorithm estimate of the friction coefficient is higher; thus a longer distance-to-go is predicted. Conversely, performance levels greater than normal are interpreted as a lower than actual friction coefficient. Thus there exists a family of curves for the acceleration vs air-speed relationship, each curve being associated with a particular *effective friction coefficient* which does not necessarily represent the true *coefficient of rolling friction*. These arguments generally agree with the results of other studies (eg Ref. 12,14). It should be recognised that the estimated effective friction coefficient does not necessarily remain constant during the period of a particular performance anomaly. For example, in both the incorrect flap setting and aerodynamic degradation (eg due to snow) simulations its magnitude varied gradually during ground roll[3]. In these particular cases the

234

effect became more pronounced at high speed due to the velocity squared relationship of the drag force. One disadvantage of the algorithm is that the predictions are based on the current effective friction coefficient estimate and, for example, runway conditions ahead of the airplane may not be properly accounted for. On a slush covered runway the contaminant depth is not usually uniform along the entire runway length and the slush drag varies as the square of the speed. Ref. 14 attempts to account for this latter effect.

The conversion of (flight manual) V_1 and V_R (CAS) to true airspeeds is a function of ambient temperature[3] and is a necessary step to establish integration limits for the distance-to-go predictions. Thus for erroneous temperature inputs an error component is introduced in these distance estimates, even if the effective friction coefficient concept responds to incorrect temperature data. eg For the dry runway case a temperature underestimation of 10 K gives rise to an additional error of 3.8% when estimating l_{vRm}[3].

The windspeed estimator was extremely beneficial and ensured that unexpected changes in wind conditions were accounted for. In addition, the use of actual runway profile data (as opposed to effective gradient) enhanced the accuracy of all predictive computations[3].

For the IRS/GSS hybrid scheme the Kalman[3] or Complementary[12] Filters can be exploited as state estimators. Fig. 20 shows how closely the Kalman Filter can track the true values. If either the GSS or IRS function fails completely then the system reconfigures to utilise a simple filter to process the remaining signal. As an example consider failure of the GSS function at brake release. For the dry runway case above, l_c and the velocity signal are in error by almost 100 m (4.8%) and 5 m/s (6%) respectively at rotation speed. Furthermore, this gives rise to inferior windspeed estimates which are dependent on accurate signals from the inertial velocity reference. Inevitably the accuracy of all predictive computations degrades, eg the error component introduced in estimating S_{v1} grows to 90 m (9.5%) for the dry runway scenario. The effective friction coefficient (and thus the distance-to-go estimate) is also less accurate because the acceleration term in Equation 22 inherently includes errors, eg accelerometer bias. Results also indicate that in the single sensor configuration the algorithm is able to account for performance anomalies (less accurately). As an example, the effective friction coefficient estimation for an engine failure is illustrated in Fig. 21. Prior to engine malfunction the implications of less accurate acceleration data are evident.

The stopping predictions have demonstrated their ability to respond to the following anomalies

- engine failure (reduction in available reverse thrust)
- tyre failure/brake failure
- runway friction characteristics (eg dry, wet, contaminated)
- change in wind conditions.

However, the empirical braking friction coefficient data adopted herein may not accurately represent the *actual* runway conditions. Perhaps the stopping distance should be displayed as a minimum length plus a likely error band. It could be argued that measurements of the effective friction coefficient during the roll after landing could be used during the next take-off if runway conditions are comparable. However, there are a number of drawbacks associated with this method, for example discrepancies introduced due to the vast difference in the level of braking force employed during a routine landing and a maximum energy RTO. As the braking friction coefficient is a function of groundspeed, it is likely that data collected during landing will not necessarily be for the correct speed range. Other discrepancies associated with factors such as pilot technique could also be introduced.

Anomalies such as

- incorrect data input (eg ambient temperature, aircraft weight, control settings)
- incorrect loading (eg excess weight)
- incorrect control setting selected by the pilot for the prevailing conditions

cannot be accounted for by the stopping algorithms implemented here. For example, with erroneous temperature data, estimates of atmospheric density and the acoustic velocity are inaccurate and thus the aerodynamic and thrust forces are incorrectly computed for the predictions. In the dry runway case, temperature underestimated by 10 K introduces an error of 3.5% in the calculation of S_{v1}.

Both the MMM and the SGTM techniques have demonstrated their ability to detect poor engine performance for a wide range of component failures [3]. As an example, the response of the EPM scheme is illustrated in Fig. 22 - 23 for two engine conditions, namely a reduction in intake efficiency (as might occur in the case of icing or foreign object ingestion) and reduced fan performance. It is evident that there is good agreement between the EPM deduced thrust and that from a full simulation of the engine equations. In addition, the capacity of the EPM to detect engine malfunctions, including those independent of EPR, by comparison of measured and reference gross thrust is highlighted.

The use of a monitor on the reference acceleration was successful in detecting significant performance deficiencies in the simulations conducted for this study. Generally, a large difference between the estimated and reference friction coefficient existed for the non-limiting take-offs. In the presence of minor performance deficiencies the critical take-off lengths indicated that the aircraft was able to continue the take-off or stop safely from V_1, but the reference acceleration monitor did not (correctly) signal a warning. For distance limited take-offs similar anomalies were immediately detected by this acceleration monitor.

The reference friction coefficient was not re-evaluated in the presence of a change in wind conditions alone. In several simulations involving adverse wind conditions the critical take-

off lengths indicated that a threat to safety existed, whereas both reference and nominal acceleration monitors did not. The acceleration monitors have been tailored to respond to only inertial performance deficiencies. The potential advantage is that in the absence of warning from other cues (eg TPIS, EPM) the pilot could deduce that the likely source of the performance deficiency was airspeed related.

The nominal acceleration monitor was able to detect anomalies such as

- engine failure/incorrect throttle setting
- tyre failure
- variations in runway friction characteristics
- incorrect data input such as ambient temperature, aircraft weight and control settings
- excess weight
- incorrect control setting
- aerodynamic degradation, eg slush impingement drag.

However, virtually all the non-limiting take-offs were considered sub-normal whilst the performance was still within acceptable limits, ie both the GO and STOP options were available. In these cases the reference acceleration monitor did not signal a warning. Fig. 24 shows the response of both schemes to an incorrect temperature input. The strength of the reference monitor is illustrated here.

As the nominal acceleration monitor is effective in detecting anomalies due to improper configuration (eg excess weight, incorrect control setting) and incorrect data input, it could be employed at low speed. It should now be clear that algorithm estimates of the effective friction coefficient cannot be used to estimate the nominal acceleration data used for acceleration monitoring. It is recommended that data input be automatic wherever possible in order to reduce pilot work-load and to minimise errors.

11.0 Conclusions

Important improvements in operational safety could result from the widespread use of *efficient* TOPMs. Type III monitors have the potential to present information that is directly related to the pilot's task during take-off. Detection of any shortfall in the performance early in the take-off run would thus not only prevent a high speed overrun, but would also aid the pilot in judging the point at which an undisturbed take-off were possible and safe.

Potential monitoring functions, algorithms and the necessary data sources have been defined for a Type III TOPM. The pre-takeoff module calculates and displays the critical take-off lengths using nominally correct data. These parameters are displayed on the basis of measured data and forward computations during ground roll. State estimators such as Kalman and Complementary Filters can be employed to establish the take-off conditions. The monitoring of engine health and acceleration performance could potentially enhance situation awareness. The scheme also attempts to warn of incorrect throttle setting. The nominal acceleration monitor can detect per-

formance anomalies immediately, but it cannot discriminate between safe and unsafe situations. It's strength lies in being able to warn of improper aircraft configuration, shortly after brake-release. The reference acceleration monitor attempts to warn of performance levels likely to result in loss of either the GO or STOP option. The effective friction coefficient algorithm ensured that the distance-to-go predictions were able to respond to a variety of anomalies including improper aircraft configuration and a change in conditions during the ground roll (eg engine health, tyre conditions, runway contamination). The stopping predictions are more difficult to solve; they do not benefit from acceleration measurements in the same way the continued take-off predictions do. Determination of the *actual* braking friction coefficient is difficult. The approved braking friction data currently presented in JAR 25 have been employed in the proposed implementation.

A widely acceptable solution to the presentation problem is crucial to TOPM success.

12.0 Recommendations

Any reliable braking friction coefficient estimation procedure would greatly enhance the accuracy of the stopping predictions.

Both simulator and real flight trials need to be conducted before satisfaction among pilots and acceptability by airworthiness authorities develop.

A disturbing feature of many overruns on aborted take-offs is the *low* braking force actually employed by the pilot. A display of the stopping distance required during an abort manoeuvre, based on actual conditions, could greatly aid pilot stopping action. An important aspect of this study would be to establish a real-time algorithm to deduce the effective friction coefficient during braking.

A case can be made to provide the pilot with assistance similar to that described above for guidance during the landing ground roll.
It is likely that a TOPM which introduces a large number of unnecessary *high speed* RTOs will not be positively accepted by pilots and airworthiness authorities. The benefits of a TOPM are dependent on its ability to improve overall safety of the take-off. Analysis must show that the probabilities of indicating a performance deficiency when none exists (*nuisance to warn*) and the rate of failing to display deficiencies when true loss of performance has occurred (*failure to warn*) are kept to an absolute minimum.

References

[1]   CAA. World Airline Accident Summary, *CAP 479*, UK Civil Aviation Authority, 1989.
[2]   SAE. Take-Off Performance Monitor (TOPM) System, Airplane, Minimum Performance Standard For, *Aerospace Standard AS 8044*, Society of Automotive Engineers, Warrendale, PA, 1987.
[3]   Khatwa R. *The Development of a Take-Off Performance Monitor (TOPM)*, PhD Thesis, University of Bristol, Department of Aerospace Engineering, January 1991.

[4] Khatwa R. Challenges for Take-Off Safety, *NLR TP 91-L*, The National Aerospace Laboratory NLR, Amsterdam, 1991.

[5] Ashford R. *Overruns on Landings and Rejected Take-Offs*, UK Civil Aviation Authority, 1984.

[6] FAA. Takeoff Performance Monitor, Approval of Flight Management Systems in Transport Category Airplanes, *Advisory Circular AC 25-15*, Federal Aviation Administration, US Department of Transportation, 1989, pp 20-22.

[7] Morris J G, Lindsay J L. Description and Preliminary Flight Investigation of an Instrument for Detecting Subnormal Acceleration During Take-Off, *NACA TN-3252*, 1954.

[8] Illingworth J K B, Hopkin H R. A Note on the Design of Take-Off Monitors, *RAE Technical Memorandum No 1AP 697 Aero 657*, 1960.

[9] Lee L R. Operational Evaluations of Sperry, Kollsman, and Oster Take-Off Monitors, and Final Conclusions Based Upon all Recent Take-Off Monitor Tests by Aeronautical Systems Division, Wright Patterson Air Force Base, Ohio, *Technical Documentary Report ASD-TDR-69-1971*, 1963.

[10] Baldwin S F. *System Design and Avionics Integration of a Takeoff Performance Monitor*, MSc Thesis, Texas Womens University, 1986. (UMI Order Number 1330775.)

[11] Cleary P J, Kelman L S, Horn R L. Aircraft Performance Margin Indicator, Boeing Company, *European Patent Appl No 85200977.8, Publ No 0166487 A2*, June 19, 1985.

[12] Srivatsan R. *Design of a Takeoff Performance Monitoring System*, DE Dissertation, University of Kansas, 1985; also published as *NASA CR-178255*, 1987.

[13] Middleton D B, Srivatsan R, Person L H Jr. Simulator Evaluation of a Display for a Takeoff Performance Monitoring System, *NASA TP-2908*, 1989.

[14] Verspay J. Take-Off Performance Monitoring System Algorithm and Display Development, *AIAA Atmospheric Flight Mechanics Conference*, New Orleans, August 1991.

[15] Wagenmakers J. Take-Off Performance Monitoring, *43rd International Air Safety Seminar*, Flight Safety Foundation, Rome, November 19-22 1990, pp 113-116.

[16] JAA. *The Joint Airworthiness Requirements*, *JAR 25 Large Aeroplanes*, The Joint Airworthiness Authorities (JAA), 1989.

[17] Khatwa R. Optimal Filtering of Sensor Signals for Take-Off Performance Monitors (TOPM), *17th Congress of the International Council of the Aeronautical Sciences (ICAS)*, Stockholm, 9-14th September 1990.

[18] Jazwinski A H. *Stochastic Processes and Filtering Theory*, Academic Press, New York, New York, 1977.

[19] Kaminski P G, Bryson A E Jr and Schmidt S F. Discrete Square Root Filtering: A Survey of Current Techniques, *IEEE Transactions on Automatic Control*, Vol AC-16, No 6, 1971, pp 727-736.

[20] Andrews A. A Square Root Formulation of the Kalman Covariance Equations, *AIAA Journal*, Vol 6, No 6, 1968, pp 1165-1166.

[21] Abbott T S. A Simulation Evaluation of the Engine Monitoring and Control System Display, *NASA TP 2960*, 1990.

[22] Khatwa R. Engine Monitors for Efficient Take-Off Performance Monitors, *2nd International Congress on Condition Monitoring and Diagnostic Engineering Management (COMADEM 90)*, London, 16-18th July 1990.

[23] SAE Committee E-33. In-Flight Thrust Determination, *SAE Aerospace Information Report (AIR) 1703*, Warrendale, PA, 1985.

[24] Hughes D L. Comparison of Three Thrust Calculation Methods Using In-Flight Thrust Data, *NASA TM-81360*, 1981.

[25] ESDU. Frictional and Retarding Forces on Aircraft Tyres, Part 1: Introduction, *ESDU 71025*, 1981.

[26] Collingbourne J. A Survey of Available Data on the Value of Rolling Resistance on Hard Runways, *RAE TM Aero-1233*, 1970.

[27] ESDU. Frictional and Retarding Forces on Aircraft Tyres, Part 2: Estimation of Braking Force, *ESDU 71026*, 1981.

[28] Horne W B. Status of Runway Sliperiness Research, Aircraft Safety and Operating Problems, *NASA SP-416*, Hampton, Virginia, October 18-20, 1976, pp 191-245.

[29] Agrawal S K. Braking Performance of Aircraft Tires, *Progress in Aerospace Sciences*, Vol 23, 1986, pp 105-150.

[30] Hainline B C. Amberg R L. Srinath S K. Prediction of Aircraft Braking Friction on Wet Runways-A look at Past and Current Research Activities, *SAE Technical Paper 831562*, Warrendale, PA, 1983.

[31] Verspay J, Khatwa R. *The Work-Station Evaluation of Three Take-Off Performance Monitor Display Types*, The National Aerospace Laboratory NLR, Amsterdam, 1992 (in preparation).

Acknowledgements

Table 1 TOPM data requirements

Ambient conditions	Ambient temperature Ambient pressure Windspeed and direction
Runway data	Runway contamination (as defined in JAR 25) Nominal rolling friction coefficient Runway profile Runway heading Runway available for rotation Runway available for stopping
Aircraft configuration and loading data	Aircraft weight Centre of gravity location Flap setting Stabiliser setting Recommended static EPR for take-off
Take-off speeds	Decision speed (V_1) Rotation speed (V_R) Lift-off speed (V_{LO}) Take-off safety speed (V_2)

Table 2 JAR 25 Wet runway braking characteristics

Groundspeed (knots)	Factor $\dfrac{\mu_{Bwet}}{\mu_{Bdry}}$
20	0.64
40	0.64
60	0.62
80	0.57
100	0.52
120	0.48
140	0.44
160	0.41

Table 3 TOPM real-time inputs

Longitudinal acceleration (IRS)
Ground speed (GSS)
TAS/CAS (ADC)
Estimated windspeed
Tyre monitor (TPIS)
Runway slope data
Throttle position
Engine exhaust nozzle pressures P_{t3}, P_{t7},
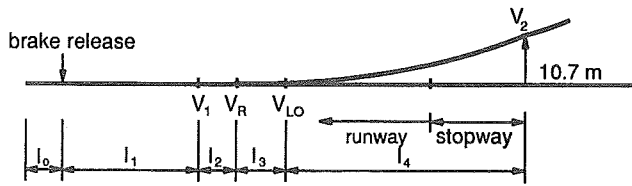
Fig. 1 Critical take-off speeds
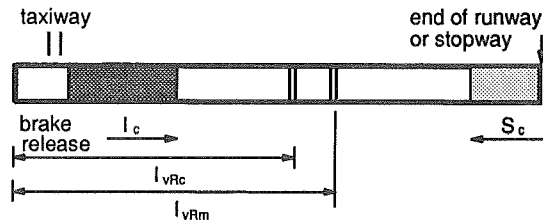
Fig. 2 TOPM predictive concept
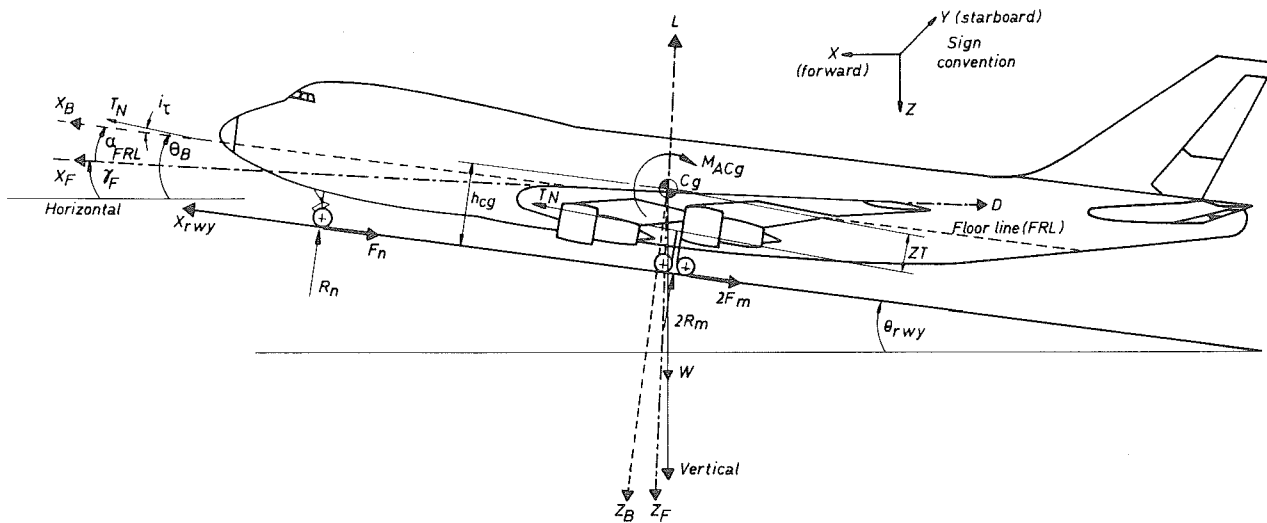
Fig. 3 Forces acting on airplane during ground roll

237
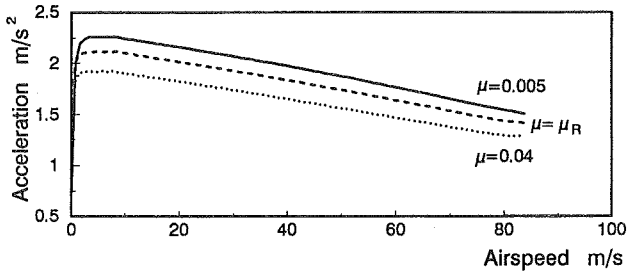
Fig. 4 Prediction of airplane acceleration performance
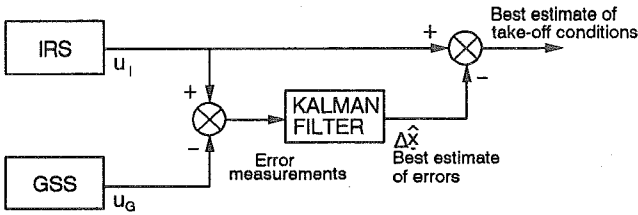
Fig. 5 Indirect feedforward Kalman Filter mechanisation
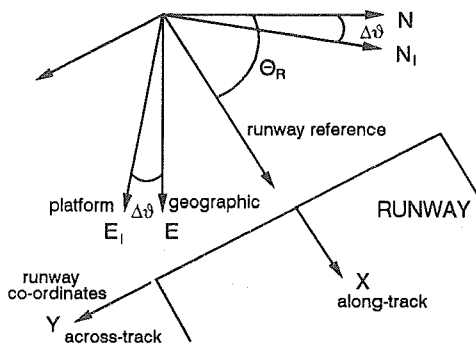
Fig. 6 Co-ordinate systems
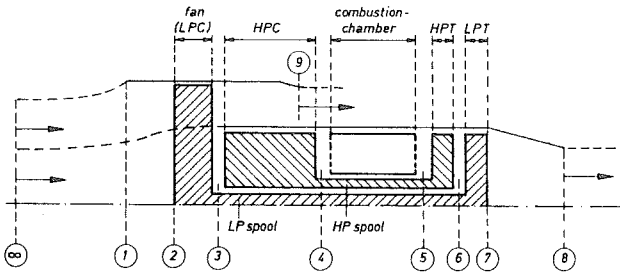
Fig. 7 Twin spool turbofan
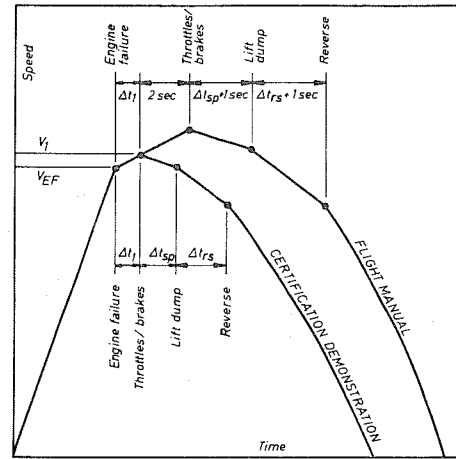
Fig. 8 JAR 25 accelerate-stop certification
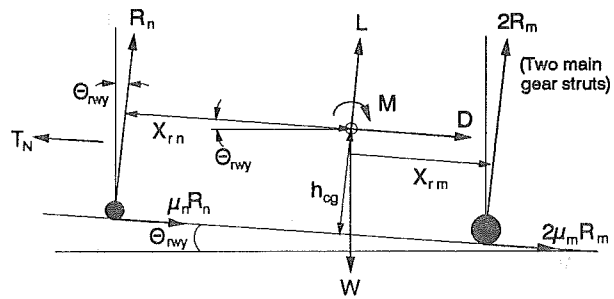
Fig. 9 Forces present during the braked roll
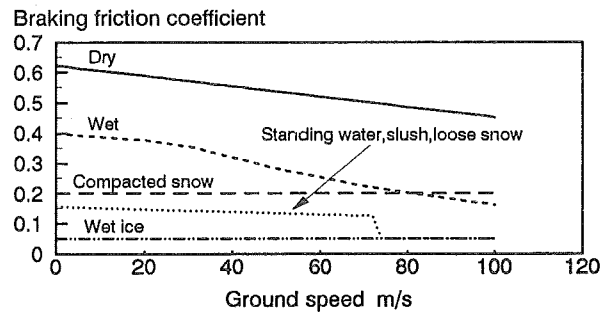
Fig. 10 Braking friction coefficients
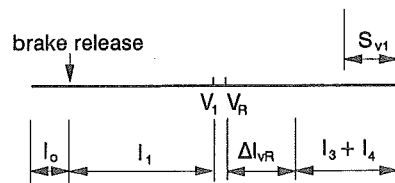
Fig. 11a $I_3 + I_4 > S_{v1}$
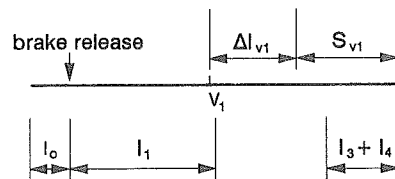
Fig. 11b $I_3 + I_4 < S_{v1}$

Fig. 11 Reference acceleration critical lengths

238
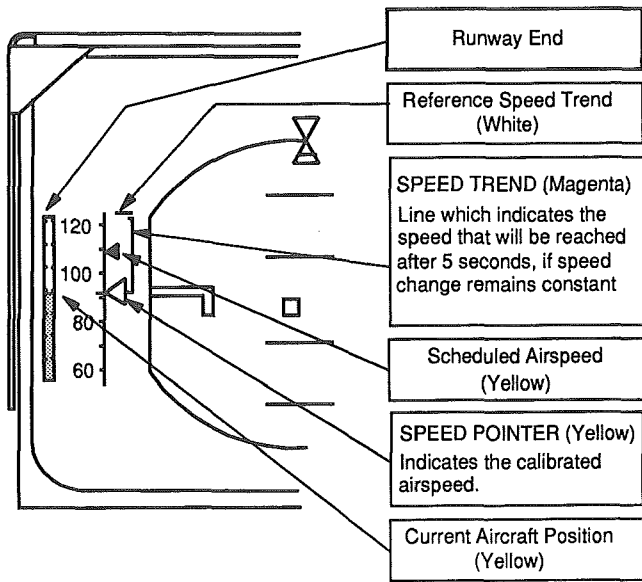
Fig. 12 Type I TOPM
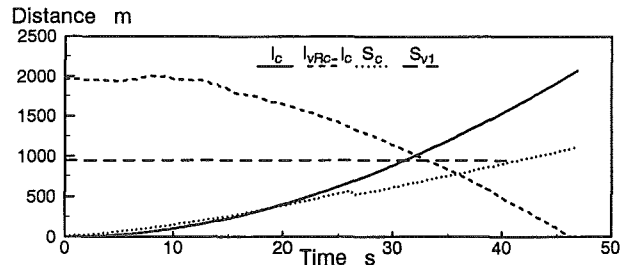
Fig. 17a Estimation of critical take-off lengths
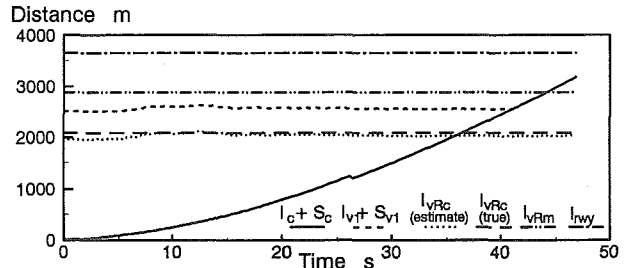
Fig. 17b Comparison of critical take-off lengths
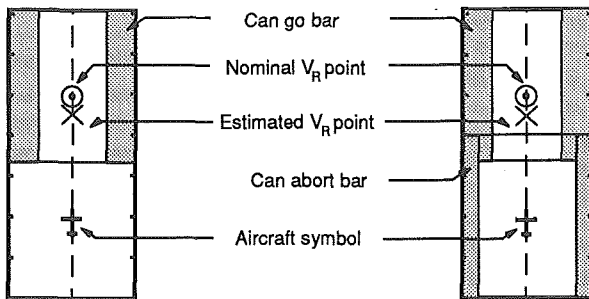
Fig. 13 Type II TOPM   Fig. 14 Type III TOPM
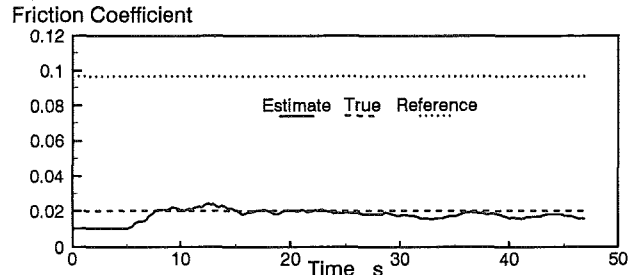
Fig. 17c Comparison of friction coefficients
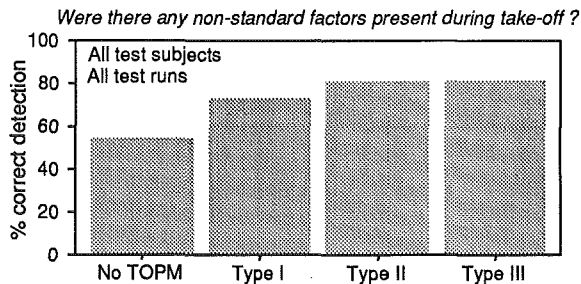
Fig. 15 Comparison of non-standard performance detection
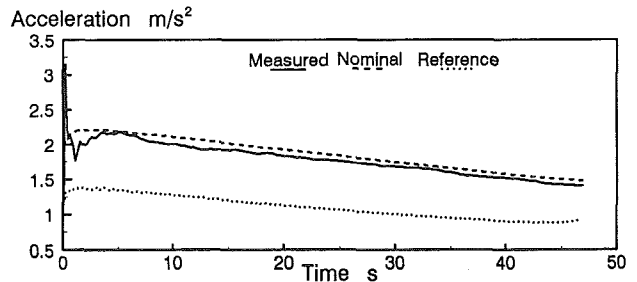
Fig. 17d Comparison of accelerations

Fig. 17 TOPM response to dry runway conditions
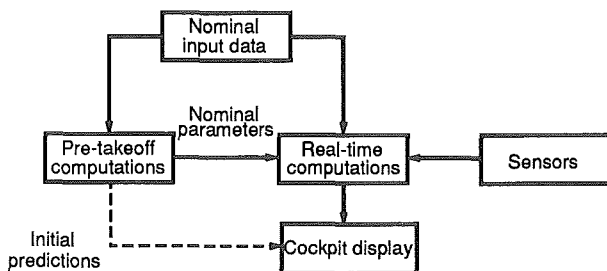
Fig. 16 TOPM block diagram

239
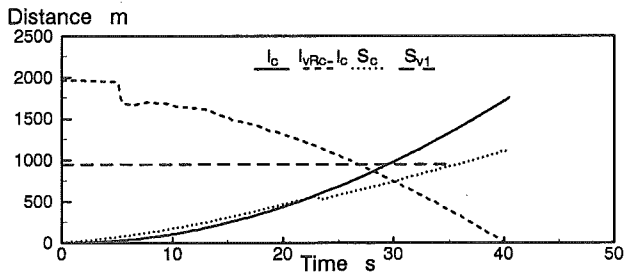
Fig. 18a Estimation of critical take-off lengths
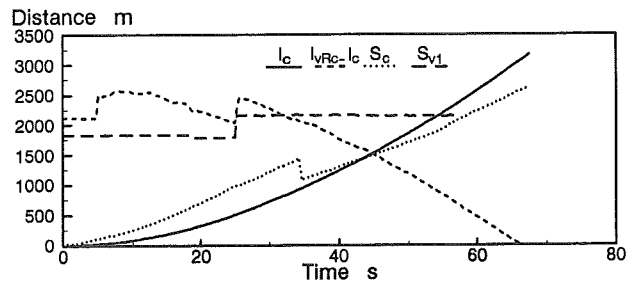
Fig. 19a Estimation of critical take-off lengths
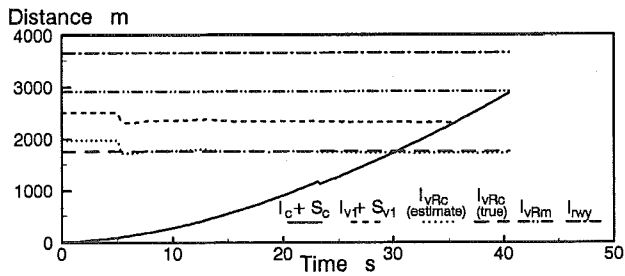
Fig. 18b Comparison of critical take-off lengths
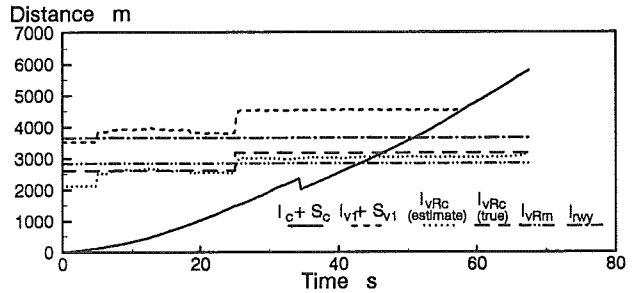
Fig. 19b Comparison of critical take-off lengths
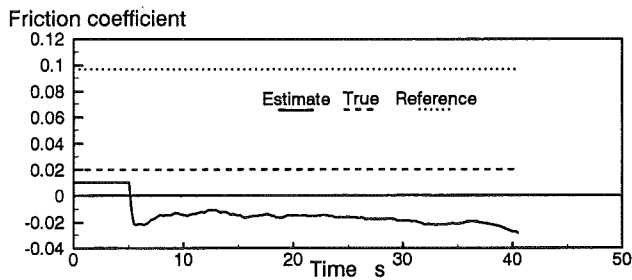
Fig. 18c Comparison of friction coefficients
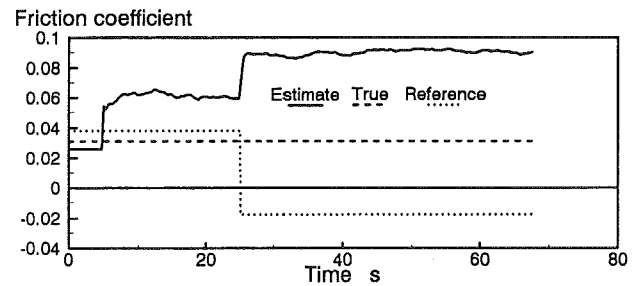
Fig. 19c Comparison of friction coefficients
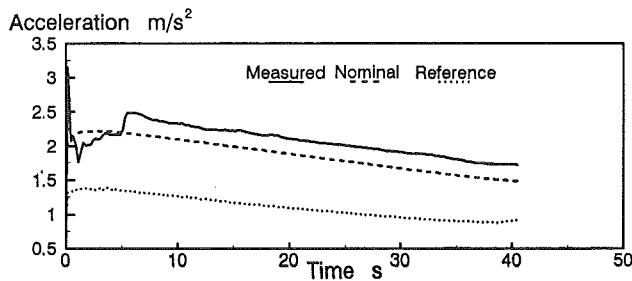
Fig. 18d Comparison of accelerations
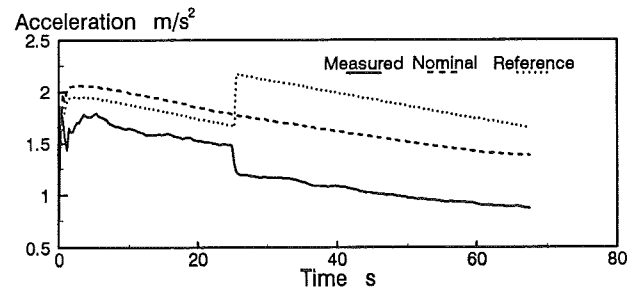
Fig. 19d Comparison of accelerations

Fig. 18 TOPM response to thrust setting too high
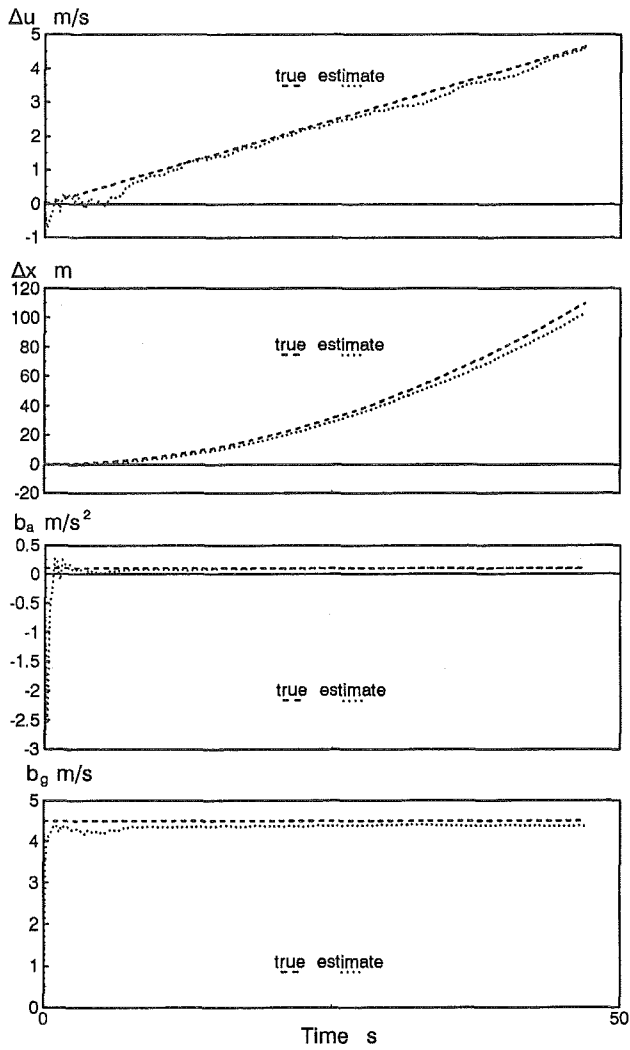
Fig. 19 TOPM response to excess weight and engine failure

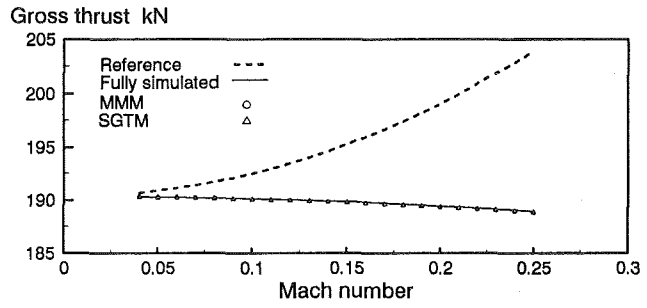Fig. 20 Actual and estimated measurement errors

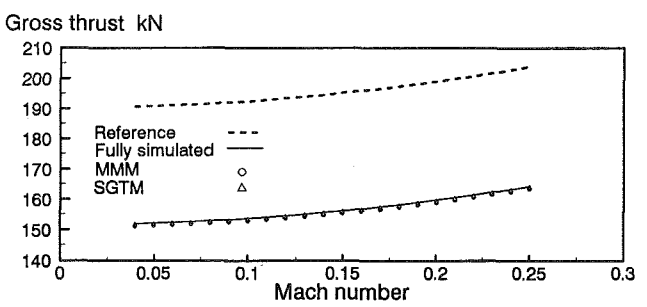Fig. 22 In-flight thrust for sub-standard intake performance
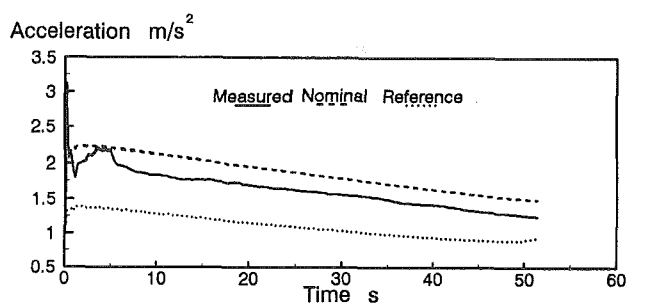

Fig. 23 In-flight thrust for sub-standard fan performance

Fig. 24 Comparison of accelerations: Incorrect temperature input

Fig. 21 Friction coefficient estimation: GSS and engine failure

241